J. Exp. Mar. Biol. Ecol., 158 (1992) 1–36

JEMBE 01751

Electron probe microanalysis of fish otoliths – evaluation of techniques for studying age and stock discrimination

John S. Gunn[a], Ian R. Harrowfield[b], Craig H. Proctor[a] and Ronald E. Thresher[a]

[a] *CSIRO Division of Fisheries, Hobart, Tasmania, Australia*; [b] *CSIRO Division of Mineral Products, Port Melbourne, Victoria, Australia*

(Received 14 August 1991; revision received 19 November 1991; accepted 18 December 1991)

Abstract: Electron probe microanalyzers fitted with energy-dispersive (ED) and wavelength-dispersive (WD) X-ray spectrometers are the standard instruments for measuring microscale differences in the chemical composition of the calcified tissues of fishes. We review the principles of using these spectrometers, detail procedures for preparing otoliths for microanalysis, and compare the accuracy and sensitivity of the two instruments. ED systems on electron probes are prone to produce spectral artifacts, peak overlaps and difficulties in modelling nonlinear backgrounds. Current generation ED systems do not, therefore, appear suitable for quantitative analysis of trace elements (< 5000 ppm) in otoliths. For the species we examined, WD systems could measure six elements (Ca, Na, Sr, K, S and Cl) accurately and precisely to levels of several hundred ppm. However, electron probes operating at the beam powers required for WD analysis damage otoliths, causing pitting and chemical change, which increases measurement errors. This damage and the consequent loss in data quality vary directly with the power density of the electron beam, which, in turn, determines in part the rate of data acquisition. Use of a WD spectrometer to analyze otoliths, therefore, requires making a trade-off between acquisition time and data quality, which has to be evaluated against the magnitude of natural variability in the composition of the otoliths of each species studied. In the species we examined, we concluded that beam power densities $> 3\ \mu W \cdot \mu m^{-2}$ resulted in unacceptable levels of specimen damage.

Key words: Life history scan; Microanalysis; Otolith

Introduction

The calcified tissues of teleosts – their bones, scales and otoliths – are composed of a calcium carbonate-protein or calcium phosphate-protein matrix into which are bound a large number of microconstituents, elements that are either incorporated into the protein structure or replace calcium, carbon or phosphorus in the crystalline component of the matrix (Carlstrom, 1963; Degens et al., 1969). As early as 1967 (Fisheries Agency of Japan, 1967), preliminary studies suggested that the quantitative analysis of these microconstituents, or trace elements, could provide information on population structure

Correspondence address: J.S. Gunn, CSIRO Division of Fisheries, PO Box 1538, Hobart, Tasmania 7001, Australia.

Order of authorship alphabetical.

and movements. This suggestion was based on two assumptions and a hypothesis. The assumptions are: (1) that the calcified tissues of fish, with few exceptions, are not susceptible to dissolution or resorption; and (2) that growth continues throughout life. If these assumptions are correct, calcified tissues are permanent records of the influence of endogenous and exogenous factors on their calcium-protein matrices. The hypothesis is that genetic differences between populations or differences in the environments to which each population is exposed affect the incorporation of trace elements in calcified tissues, which results in chemical compositions specific to each. An extensive fisheries literature supports the initial assumptions for otoliths, which are the calcified structures we have dealt with. The working hypothesis also appears reasonable, given an extensive literature on invertebrates that relates differences in the composition of, for example, mollusc shells and coral skeletons (calcium carbonate matrices similar to those in fishes) to a range of environmental and physiological conditions (Thompson & Livingston, 1970; Weber, 1973; Houck et al., 1977; Buchardt & Fritz, 1978; Smith et al., 1979; Rosenberg, 1980; Schneider & Smith, 1982).

Since 1967, measurements of trace elements in calcified tissues of fishes have been used in three areas of fisheries science. First, as indicators of pollution, principally by heavy metals (Papadopoulou et al., 1978, 1980; Johnson, 1989). Second, as a means of determining the ages of fishes, through analysis of either the rates of decay of ^{210}Pb and ^{226}Ra (Bennett et al., 1982; Campana et al., 1990) or the concentrations of isotopes or elements thought to vary seasonally as a function of water temperature, e.g., oxygen isotopes (Devereaux, 1967; Degens et al., 1969; Mulcahy et al., 1979; Radtke, 1984 a & b; Radtke et al., 1987), iron (Gauldie & Nathan, 1977; Gauldie et al., 1986), phosphorus/strontium ratios (Calaprice, 1985) and strontium/calcium ratios (Radtke & Targett, 1984; Radtke & Cailliet, 1984; Radtke, 1987, 1989; Radtke & Morales-Nin, 1989; Radtke et al., 1989). And third, as an indicator of stock or sub-population identity (e.g., Klokov & Frolenko, 1970; Calaprice, 1971, 1983, 1985; Calaprice et al., 1971, 1975; Bagenal et al., 1973; Behrens Yamada et al., 1979; Lapi & Mulligan, 1981; Mulligan et al., 1983, 1987; Edmunds et al., 1989). The analytical techniques used in these studies have included atomic absorption spectrophotometry (Gauldie & Nathan, 1977; Gauldie et al., 1980), X-ray fluorescence spectro(photo)metry (Calaprice, 1971, 1985; Calaprice et al., 1971, 1975; Mulligan et al., 1983; Behrens Yamada et al., 1987), neutron activation analysis (Fisheries Agency of Japan, 1967; Papadopoulou & Moraitopoulou-Kassimati, 1977; Papadopoulou et al., 1978, 1980), X-ray diffraction (Morales-Nin, 1987), radiochemical analysis (Bennett et al., 1982), stable isotope analysis (Radtke, 1983, 1984a; Radtke et al., 1987), proton-induced X-ray emission spectrophotometry/proton-nuclear microprobe analysis (Calaprice, 1985; Gauldie et al., 1986), energy-dispersive X-ray electron microanalysis (Lapi & Mulligan, 1981; Mulligan et al., 1987) and wavelength-dispersive X-ray electron microanalysis (Radtke & Cailliet, 1984; Radtke & Targett, 1984; Radtke, 1987; Kalish, 1989; Radtke & Morales-Nin 1989; Townsend et al., 1989). That no single technique has been universally adopted reflects the developing nature of the field and the diversity of

research objectives. Moreover, to date there has been no comprehensive analysis of the advantages and disadvantages of each technique for analyzing the calcified tissues in fishes.

We began experiments in 1987 with a view to using ontogenetic variations in the chemical composition of fish otoliths as an indicator of movement/migration patterns. Acquiring such data dictated the use of a probe microanalyser, which could be scanned along a growth axis. Four probe microanalysers are suited for such studies – electron, proton, ion beam and laser ablation probes. The relatively low cost, easy availability and apparently adequate sensitivity of electron probe microanalysers, based on the literature and the results of our pilot studies, suggested we focus our initial efforts on determining their suitability for analysis of otolith composition.

To acquire and interpret the ontogenetic data obtained with a probe microanalyser, two things are required. First, we needed a method for accurately sectioning otoliths along equivalent growth axes in different individuals, while providing the flat, smooth surface the microanalysers require. And second, we needed to make an informed choice between the two available electron probe techniques (energy-dispersive X-ray spectroscopy [ED] and wavelength-dispersive X-ray spectroscopy [WD]) for analyzing of the aragonite matrices of fish otoliths.

This paper describes the techniques we developed to prepare otoliths for analysis on an electron microprobe, discusses the strengths and weaknesses of ED and WD spectrometers in such analyses, and considers the problems and the compromises involved in acquiring data.

Description of Techniques and Experimental Results

Preparation of otoliths for electron probe microanalysis

Procedures for sectioning and polishing fish otoliths have been described previously by Pannella (1980), Neilson & Geen (1981), Radtke & Targett (1984), Karakiri & Westernhagen (1988), and Kalish (1989), among others. Relevant studies involving probe microanalysis have dealt with the requirements for single-point analyses; we describe our procedures in detail because they were developed for full life-history scans (sequential analysis at points along the complete growth axis of an otolith, and hence throughout the life of a fish) and because the standards of specimen preparation affect the quality of the data. This section is not a review of the field nor meant to imply that our techniques are superior to those described elsewhere. Rather it summarizes the procedures we have found necessary and sufficient to produce specimens of high enough quality for electron probe microanalysis.

Cleaning and storage of otoliths

After extraction, we cleaned each otolith of adhering tissue using fine forceps and a soft bristled brush in millipore-filtered distilled water. The otoliths are then dried in an

oven at 40–45 °C for a minimum of 6 h. Otoliths taken from specimens stored in ethanol should be transferred into progressively dilute solutions of ethanol prior to drying, to prevent rapid dehydration and consequent fracturing. After drying, the otoliths are stored in small polyurethane capsules (20 mm long, 9 mm diameter, normally used for embedding purposes in transmission electron microscopy) in a moisture-free cabinet or under vacuum.

Embedding, sectioning and mounting

The procedure for embedding and sectioning sagittae that we used is as follows: (1) An accurately scaled diagram of the distal surface of the otolith is made with a camera lucida on a stereo-dissecting microscope. The position of the primordium must be accurately marked on the diagram. (2) With the otolith oriented dorso-ventrally, the desired plane of analysis in our experiments ran anterior-posterior at the level of the primordium. To achieve a section encompassing this plane, the otolith is fixed firmly upright on its ventral edge to the base of an embedding mould with a drop of quick-drying epoxy resin. We used flat-bottomed polyurethane vials, in diameter slightly greater than the length of the otolith, as moulds. The mould is then filled with a

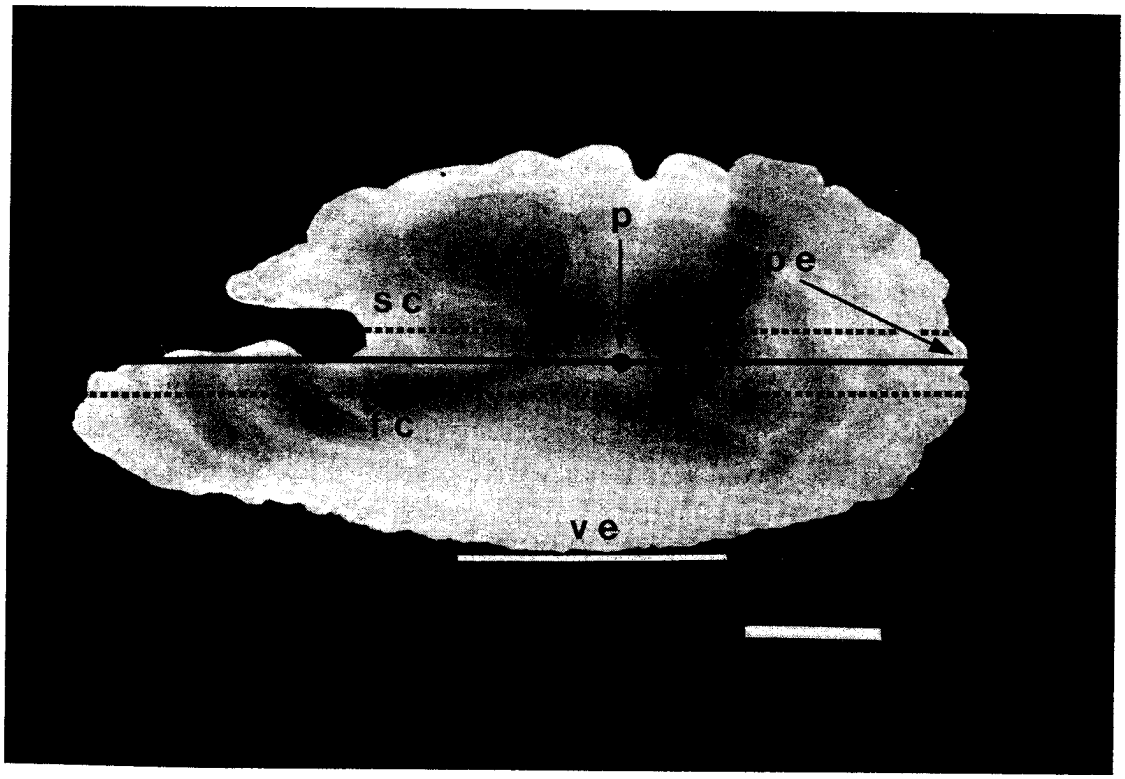

Fig. 1. Distal view of a *N. macropterus* sagitta, showing position of first cut (fc) and second cut (sc) taken to provide a section that includes primordial region (p) and full growth axis to posterior extremity (pe). Solid line at ventral edge (ve) of otolith illustrates region of otolith that is glued to base of mould. Scale bar, 2 mm.

hard-setting polyester resin. (See Mulligan et al. (1987) for a discussion of the desirable qualities of resin used for this purpose.) (3) The otolith is sectioned with a diamond-edged saw blade (350 μm thickness) on a rotary saw. The level of the first cut is determined from measurements made from the scaled diagram in Step 1. Usually, we made the first cut 250 μm below and parallel to the desired plane of analysis. A second cut, 250 μm above the plane of analysis, produces a section 500-μm thick that contains a complete growth axis (Fig. 1). Ultimately, the thickness of the finished section depends on the accuracy of the scaled diagram and the precision of the cutting equipment. We also found that a small graphite-pencil mark on the distal face of each otolith that indicated the level of the primordium aided accurate sectioning.

Preparatory to grinding, we mounted the section onto a glass round (0.8–1.0 mm thick, diameter slightly greater than the section) with a quick-set epoxy resin, so that the side of the section closest to the primordium is against the glass. In thin sections (<300 μm), the primordium can usually be seen with transmitted light microscopy. In thicker sections, or where the primordium is not close to either side, the section is affixed to the glass round with paraffin wax. This wax can be melted, which allows reversing the position of the otolith and grinding both sides of the section close to the plane of the primordium.

Grinding and polishing

Sections have to be ground to expose the growth axis, and then polished to produce the flat, featureless surface required for electron probe X-ray microanalysis. Surface defects can affect data quality by altering the absorption patterns of measured X-ray intensities in ways difficult to quantify (Potts, 1987). We grind the otolith by hand, with the section (on the glass round) held in a suitable grinding tool (an adaptation of that described by Naney, 1984), using 2400 grade silicon carbide wet/dry paper. Final polishing is done using progressively finer grades of diamond paste (6–0.5 μm) and/or aluminum oxide powders or pastes (e.g., Linde B, 0.5 μm) on a lapping machine. It is critical that the section and grinding/polishing tools be ultrasonically cleaned between all stages of the process, as cross-contamination of media inevitably scratches the surface of the section, which can adversely affect data quality. We discard data affected by surface irregularities, identified as such by inspection of the scan point "scars" after analysis.

After polishing, the section is ultrasonically cleaned of residual polishing compounds, using ethanol or some other suitable solvent, and then stored in a moisture-free environment, preferably under vacuum.

Coating

Non conductive specimens, such as otolith sections, must be coated with a thin conductive layer to prevent charge build-up. The coat should be of uniform and known thickness, as absorption of X-rays by the coating affects the accuracy of an analysis,

particularly when counting long wavelength X-rays. We use a carbon coat of 250–300 Å thickness on all standards and specimens. Prior to coating, the specimen is heated under vacuum at 80 °C for 5–10 min to remove residual moisture, particularly from pits and cracks, to prevent bubbling and flaking of the coat during analysis. After coating, the specimen is held under vacuum until it is inserted into the probe.

CHOICE OF AXIS FOR ANALYSIS

Species-specific differences in otolith structure to a large extent determine the choice of section required to expose a complete growth axis. The sagitta of tuna *Thunnus maccoyii* Castelnau (Scombroidei), for example, has a long rostral process and a deep sulcus. For life-history scans of these otoliths, a section that runs from the primordium to the posterior ventral tip of the otolith provides a long, uninterrupted growth axis along which a complete life-history scan can be run. However, due to the shape of the section and the asymmetrical patterning of the growth axes, programmed probe analysis requires a mapped series of scan lines that track through the curve apices (Fig. 2). In contrast, the finished section from the sagitta of morwong *Nemadactylus macropterus* Gill, a demersal cheilodactylid from temperate Australian waters, is more nearly linear

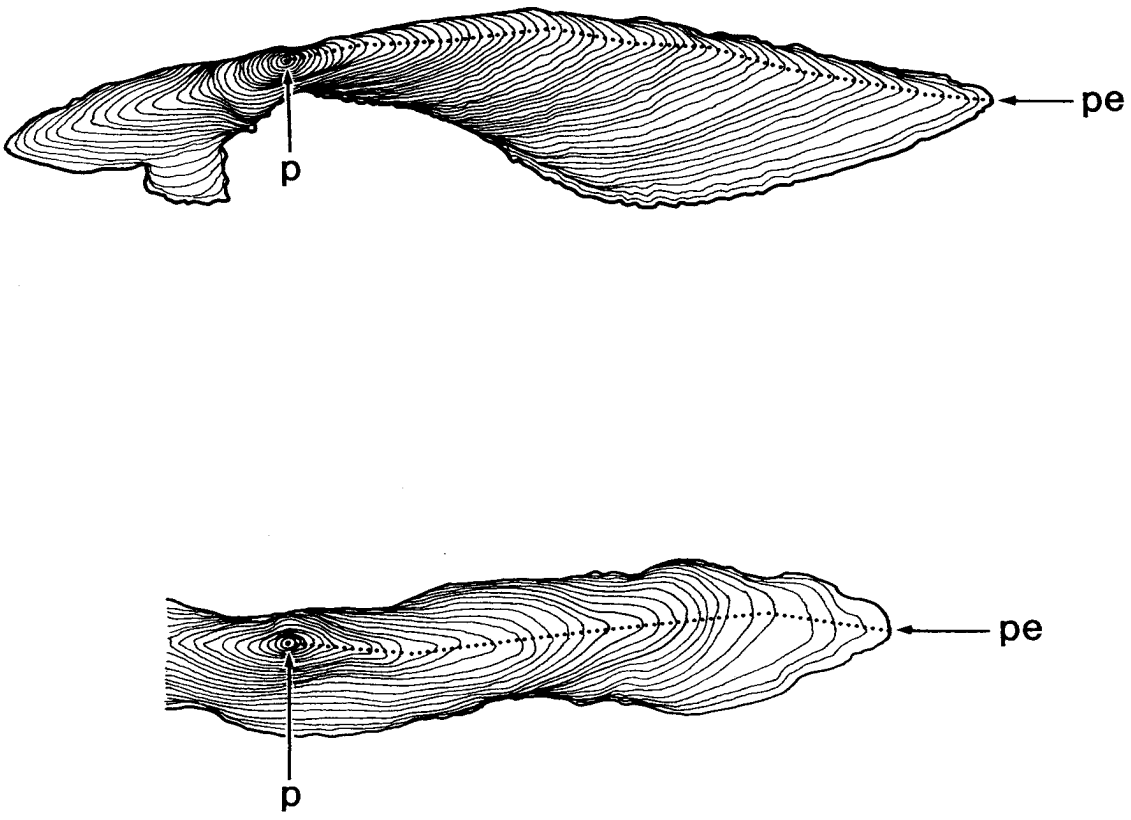

Fig. 2. Diagrammatic representation of a prepared section from a *T. maccoyii* sagitta (upper figure) and a *N. macropterus* sagitta (lower figure) showing position of programmed series of electron probe analyses through full growth axis, from primordium (p) to posterior extremity (pe).

and may require only one or two such lines (Fig. 2). In both species, tracking through the curve apices results in data acquired along the fastest growth axis. This not only provides the best resolution of growth-dependent variation in composition, but also constitutes a standard scan axis for all individuals, which facilitates comparisons among them.

Comparison of ED and WD X-Ray Spectrometers for Electron Probe Microanalysis of Otoliths

THEORETICAL CONSIDERATIONS

An electron probe microanalyser is essentially a scanning electron microscope to which is fitted one or more X-ray detection devices capable of recording X-ray intensity as a function of the photon wavelength or energy. There are two types of X-ray spectrometer on electron probe microanalysers: the energy-dispersive (ED) spectrometer and the wavelength-dispersive (WD) spectrometer. The operation, advantages and disadvantages of each for the acquisition of data from otoliths are now briefly discussed. More detailed treatments of X-ray spectrometry, data acquisition and, in particular, explanations of matrix corrections can be found in the literature on electron probe microanalysis (EPMA) (e.g., Reed, 1975; Heinrich, 1981). For readers not familiar with the field, Goldstein et al. (1981), Moreton (1981), Russ (1984) and Morgan (1985) provide excellent introductions.

The ED spectrometer is a multichannel device that, in normal operation, acquires a spectrum of a broad range of X-ray energies. When an X-ray photon enters the spectrometer's detector (a piece of cooled silicon or germanium), its energy is converted into an electrical pulse with an amplitude proportional to the energy. According to this amplitude, the number in a particular memory location in a computer is incremented by 1. Commonly, the photon energies are mapped into 1024 memory locations or channels and then a spectrum, or energy histogram, of the photons that have entered the detector over a specified period is displayed. The vertical axis of the histogram represents the number of photons per channel and the horizontal axis is usually calibrated in energy units of thousands of electron-volts (keV).

In contrast to the ED system, a WD "spectrometer" is, strictly speaking, a monochromator or a single-channel analyser – it allows photons of only one, very limited, range of wavelengths to pass into its detector. The mean wavelength of this range is set by adjusting the angle at which the photons impact onto a diffracting crystal of a known plane spacing. If a spectrum is required, the crystal is serially and discretely scanned over the appropriate range of angle. At each setting, a count is made of the photons whose wavelength satisfies the constructive interference conditions defined by the crystal plane spacing and the chosen angle of incidence. Acquisition of a broad spectrum using a WD system is possible but very time consuming, so is seldom performed.

The fundamental difference between the two detectors is that the ED spectrometer is an electronic device that processes X-ray energies over an entire spectrum, whereas the WD spectrometer has a narrow operating range defined by the mosaic properties of the diffracting crystal and the width of the counter slit. This fundamental difference has two important consequences.

First, superficially the ED spectrometer is much more efficient at counting the photons entering its input aperture than is the WD spectrometer; because it processes the entire spectrum simultaneously it can acquire data on a range of elements much more quickly than can a WD spectrometer, which collects data on only one element at a time. For this reason, most WD-based EPMAs incorporate three or four spectrometers, each with a crystal with a different lattice plane spacing, among which the task of measuring peaks and backgrounds can then be shared. However, the electronic pulse processing circuitry in an ED spectrometer is much slower than the equivalent circuitry in a WD spectrometer: the former must amplify very accurately small signals from its semiconductor-based detector, whereas the latter only has to count the pulses whose range has been set by the physical properties of the detecting crystal. The high input rates of X-ray photons achievable in a WD spectrometer would saturate ED pulse electronics. As a consequence, WD spectrometers can operate efficiently at primary beam currents an order of magnitude higher than is practical for an ED spectrometer. The net effect is that an electron probe equipped with WD spectrometers can collect, in a given time, many more X-rays for analysis of a particular element than one equipped with a single ED spectrometer, which affects the counting statistics and hence the precision and resolution of the analysis.

Second, electronic amplification in an ED spectrometer also affects data quality and procedures for data processing. In an ED spectrometer, the energy conversion of an X-ray photon into an electrical pulse involves a degree of uncertainty due to random physical events. If sufficient conversions are made, the magnitude of the pulse is normally distributed about a mean value. Because of this conversion uncertainty, a monoenergetic flux of X-rays typically produces a peak 100 eV or more wide when measured by an ED spectrometer. By comparison, the peak on a WD spectrometer is only a few eV wide, since it is set independently of the electronic processing by the lattice structure and orientation of the diffracting crystals.

This difference between the spectrometers affects the way the data are processed. The spectra analysed by both spectrometers are generated, in the main, from photons arising from two processes. First, photons are emitted when atoms excited by the primary electron beam return to their ground state; these photons are referred to as "characteristic X-rays", have well defined energies or wavelengths, and appear in the generated spectrum as narrow peaks. Their position and magnitude depend on the element, the electron shell(s) stimulated and the number of primary electrons. The second source of photons is the deceleration of electrons in the primary beam by the target. This deceleration produces a low, continuous background X-ray spectrum, known as the "bremsstrahlung" (braking radiation). The narrow "characteristic X-ray peaks" sit on

this background. The relationship between these peaks and the background differs between spectrometers, due to the way the data are processed. Electronic noise associated with data processing in ED spectrometers results in relatively broad peaks, again typically > 100 eV wide, that are rarely > 3–20 times higher than the local background. In contrast, the narrow peaks in a WD spectrometer rise 30–300 times above the background.

The first step in analyzing the spectrum obtained by EPMA is to remove the background and measure the magnitudes (i.e., height or area) of the peaks. This can be difficult with an ED spectrometer and is prone to error. The wide peaks in an ED spectrum often overlap and sit on relatively wide, often very nonlinear regions of the background, all of which reduces the precision of the estimates (for background "stripping" procedures in ED spectrometry, see Ware and Reed, 1973; Schamber et al., 1977; Statham, 1977; Ware, 1981). In contrast, removing the background from WD peaks is usually simple. The background on one or both sides of the peak is measured, the value directly under the peak is calculated by extrapolation or interpolation and this value is subtracted from the peak ordinate. The implicit assumption of background linearity is generally warranted because of the narrow range of the background spectrum.

The differences between the spectrometers in peak-to-background ratios and the accuracy with which the background can be estimated critically affect the precision of measured concentrations and minimum detection limits. The confidence interval for concentrations measured by EPMA can be found by solving for the roots of the quadratic expression given by Ancey et al. (1978). If one assumes that the background in the standard is negligible relative to the peak count rate, the percentage error (E) in the measured concentration can be expressed as:

$$E = 100 \frac{\sqrt{\left(n_p + \frac{n_b}{a^2}\right)\chi^2}}{n_p - \frac{n_b}{a}}, \qquad (1)$$

where n_p is the total number of counts collected in the peak channel(s); n_b is the total number of counts collected in the background channel(s); a is the ratio of background to peak counting time; χ^2 is determined by the confidence level required. For example, at 95% confidence it is 3.84.

If this relationship is rewritten in terms of the difference between the peak and background counts, N_p, i.e., $(n_p - n_b)$, and the value of a is 1 (which is often the case when measuring low concentrations), then:

$$E = 100 \sqrt{\frac{1}{N_p}\left(1 + \frac{2n_b}{N_p}\right)\chi^2}. \qquad (2)$$

That is, the percent measurement error decreases as both the absolute difference and the ratio between peak and background count rates increase. As both absolute and relative differences between peak and background count rate are higher on a WD spectrometer than on an ED spectrometer, the former is more precise. As might also be expected, the detectable concentrations can also be smaller for the WD spectrometer than for the ED spectrometer. Minimum detection limits for WD spectrometers are typically in the range of a few hundred ppm, whereas those on an ED spectrometer are typically an order of magnitude higher and, in extreme instances, can be as high as 1% by weight (Statham, 1981, 1982).

EXPERIMENTAL COMPARISONS

To test the relative utility of ED and WD spectrometers when used in EPMA for analysing elemental variations in otoliths, we compared life-history scans of the same otolith collected by means of a beryllium-window silicon ED spectrometer and a WD spectrometer. The otolith used was from a morwong *Nemadactylus macropterus*. The comparison is based on two closely spaced, parallel paths along the main growth axis of the otolith.

The ED scans were made on a LINK SYSTEMS 860 Series II ED spectrometer fitted to a JEOL JSM 25 scanning electron microscope. The take-off angle of the ED detector was 25° and the beam current was 5 nA, giving an overall output count rate of 3200 counts $\cdot s^{-1}$ (cps) at a dead time of 28% (time constant 20 μs). This is the highest practical output count rate of this model of ED spectrometer for quantitative analytical work. The counting time ("live time") was 240 s, giving a real total counting time very close to that for the WD scans. In this live time, over 750000 counts were accumulated. Concentrations were determined using the Sr L, Na K and K K series of lines. Spectrum processing to remove the background and to extract k ratios was by the filtered least squares method (Statham, 1977), in which "top-hat filtering" is applied to the spectrum. This method is widely used, giving, in general, excellent results when measuring concentrations as low as 0.5% by weight.

The WD scan was made on a CAMECA "CAMEBAX" electron microprobe at a beam current of 25 nA at 15 KeV and a counting time of 90 s (60 s on peak and 30 s on background) at each point. Three spectrometers were used simultaneously, set, respectively, to the Sr L_α, Na K_α and K K_α lines.

The results of the comparison are given in Fig. 3. For all three elements tested, both the mean and the variance of estimated concentrations differed significantly between spectrometers. The much higher variance on an ED spectrometer is due to low peak-to-background ratios and low count rates that can be achieved with this spectrometer for all three elements. In the case of Sr, the scatter is also the result of errors in mathematically stripping a strongly nonlinear background. The problem is illustrated by examining the region of the ED spectrum for strontium-free calcite several keV either side of the Sr L peak (Fig. 4). Despite the absence of Sr, the background is far from linear. This

Fig. 3. L
circles) a

non-lin
of the l
from th
"dead
peak u
becaus
introdu
The
backgr

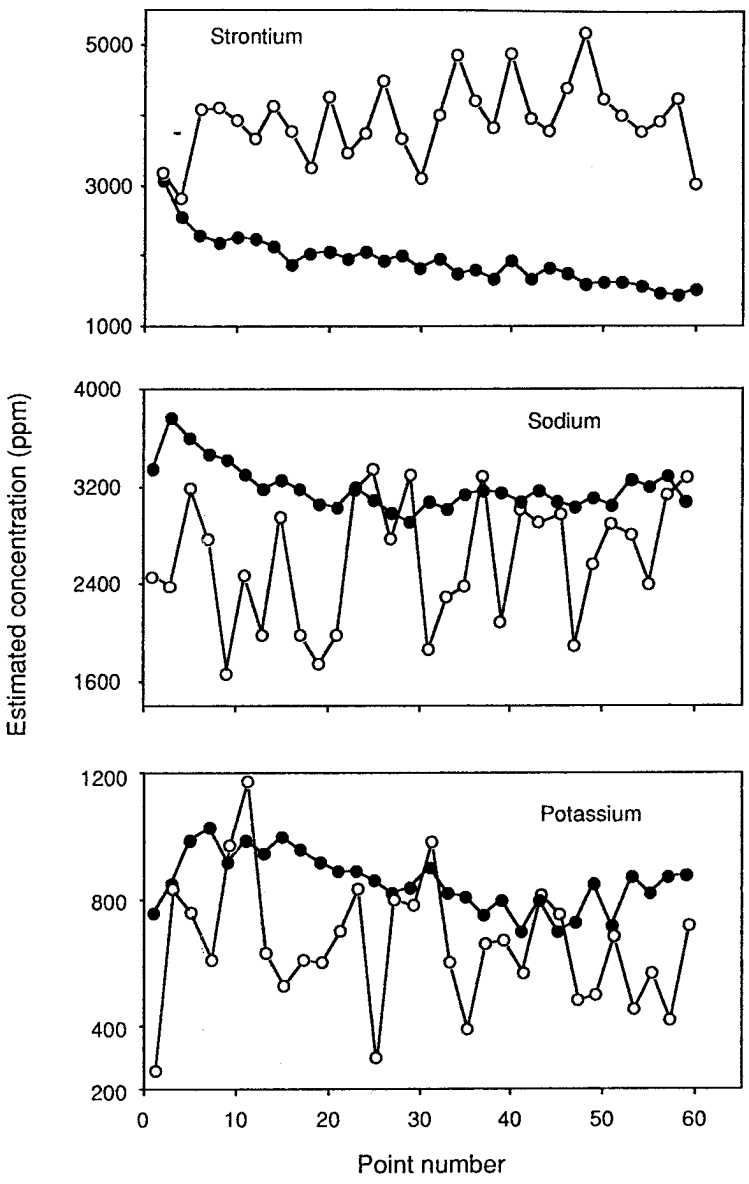

Fig. 3. Life-history scans of Sr (taken with L line), Na (K_α line) and K (K_α line) by ED spectrometer (open circles) and WD spectrometer (solid circles). Note differences in trend lines in Sr scans with two spectrometers; positive trend in ED scan is spurious, due to high noise levels.

non-linearity results, in part, from the Sr L_α line coinciding with the silicon escape peak of the large Ca K_α and, in part, from the "edge" in the background spectrum derived from the absorption of background X-rays and fluorescence of Si K_α X-rays in the "dead layer" of the detector (Statham, 1981). "Stripping" the spectrum of the escape peak using the algorithm of Reed & Ware (1972) partly reduces the problem, but also, because the modelling is not perfect, increases the noise level of the background and introduces a small systematic error.

The difference in mean values for Sr is also due in part to the very nonlinear background between 1 and 2 keV. The rapid decrease in detector sensitivity at <2 keV

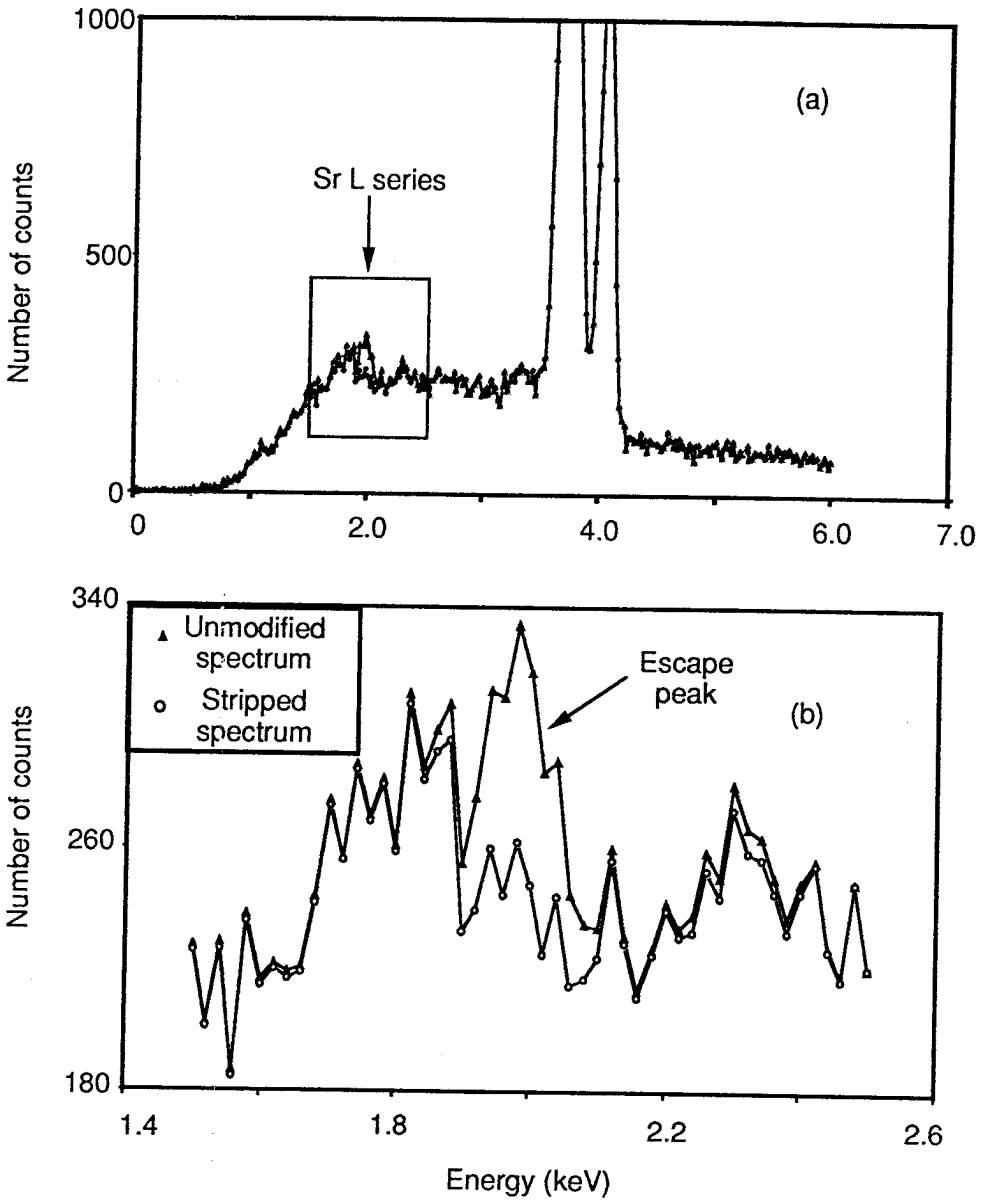

Fig. 4. ED spectra from pure calcite, $CaCO_3$ – one unmodified and one mathematically stripped of escape peak with algorithm of Reed & Ware (1972). Peak at 1.8 keV in unmodified spectrum is mostly silicon escape peak due to loss of photoelectrons from dead layer of detector. Note nonlinearity in stripped spectrum.

causes a high negative curvature which, when filtered, makes a spurious addition to any peak magnitude. As well, both the Si K_α absorption edge at 1.84 keV and the Si K_α fluorescence peak from the dead layer of the detector cause local negative curvature in the background near the Sr L_α peak that is difficult to correct (Statham, 1981). Similar systematic errors, though in this case under-estimates of concentrations due to positive background curvature, are evident in Na and K. Similar differences in accuracy between the two spectrometers are evident when run on standards for each of these elements.

Alternatives to "top-hat filtering" of the ED spectrum, which potentially could correct these errors, run into other difficulties. For example, while it may be possible to model

a reasonably accurate background curve, it is difficult to calculate the Si K_α fluorescence peak since the dead layer is not well defined (Statham, 1981). Scaling and fitting the calculated background would, inevitably, add to uncertainty in the peak magnitude. A. T. Marshall (pers. comm.) has suggested that subtracting a model spectrum taken from pure calcite from that acquired on the otolith would reduce systematic errors due to spectral artifacts. This would clearly be a better approach, since the artifacts would be similar in each spectrum. However, scaling and fitting are still required, which will add a small error.

In summary, in the ED detector tested there are systematic errors introduced by all methods of background removal in the region of the characteristic lines for Sr, Na and K. These errors are of a magnitude similar to the real concentrations of elements in the otolith. We conclude that at these concentrations, ED detectors as currently configured for use in EPMA are not sufficiently sensitive or precise to provide suitable data for our otolith-based analyses of life history scans.

WD-Based EPMA; Effects of Operating Conditions on Data Quality and Acquisition

In EPMA the kinetic energy of the primary electrons that strike the aragonite target is dissipated as heat, causing local temperatures to rise rapidly. This heat causes the calcium carbonate, which constitutes the bulk of the target, to decompose to the oxide, losing carbon dioxide. This loss reduces the target's overall mass, thereby increasing the relative abundance (weight fraction) of the remaining elements and reducing the accuracy of measurements. This problem is inherent in all EPMA, but is particularly severe in WD analysis because of the high beam currents required to accumulate sufficient counts in the spectrometers to estimate element concentrations accurately. In theory, long acquisition times using very low beam currents minimize damage and presumably measurement error. In practice, however, such long acquisition times are often not practicable (due to the cost of EPMA and the number of samples needed for population analyses) and still leave unanswered the extent to which even slight levels of target damage affect data quality. Consequently, we examined experimentally the effects of different beam conditions on measurement accuracy (and minimum spatial resolution of data points) to quantify the trade-offs involved and to determine optimal operating conditions for making life-history scans of our subject species.

Three operating parameters appeared to be of paramount significance: (1) the accelerating voltage, which determines both the excitation efficiencies for the spectral lines selected for analysis and the volume of the target from which X-rays are produced; (2) beam power density, which is the combined effects of accelerating voltage, beam current and the area scanned and which in part determines damage rates; and (3) the order in which elements (X-ray lines) are sequentially measured on the available spectrometers.

(1A) EFFECTS OF ACCELERATING VOLTAGE ON EXCITATION EFFICIENCY AND ABSORPTION OF X-RAYS

The accelerating voltage (i.e., beam energy) should be high enough to induce efficiently the most energetic selected characteristic X-ray lines for the elements being analysed, but low enough to ensure, first, that absorption correction factors for the least energetic lines are reliable when standards and specimen are dissimilar in composition and, second, that the volume of the target from which X-rays are excited is as small as possible in instances where a highly focussed probe is required. We initially tested otoliths at voltages ranging from 5 to 30 kV. 5 kV was too low to excite elements such as potassium adequately for detection, and voltages >20 kV produced very large volumes within which the X-rays were generated without a commensurate gain in measurement accuracy. We preferred to avoid large generation volumes because we occasionally need to use a nearly focussed probe in, for example, part of the otolith where growth is very slow. Hence our experimental studies were limited to the range of 10–20 kV.

We routinely measure five elements present in low concentrations, as well as Ca. Table I lists these elements, their characteristic spectral lines and the count rates (i.e., the rate of data acquisition) at these lines that would be measured on our probe at three accelerating voltages, after background subtraction and assuming a concentration of 2000 ppm by weight for each element. Values were calculated from count rates on standard materials for each line and on the ratios of the intensities on standard and aragonite targets computed with the "PAP" (Pouchou & Pichoir, 1984) matrix conversion software supplied by CAMECA. To ensure that the damage caused by heating was approximately the same at all voltages, the power dissipated in the target was arbitrarily held constant at 375 μW by adjusting the beam current. In these tests, beam size was 14 μm^2.

TABLE I

Calculated count rates for aragonite containing 2000 ppm, by weight, of various elements. Beam power is set at 375 μW.

Element and line	Count rates in Hz			Analysing crystal
	10 kV at 37.5 nA	15 kV at 25 nA	20 kV at 18.8 nA	
Na Kα	40.1	27.0	21.4	TAP
Sr Lα	32.5	40.0	40.7	TAP
S Kα	16.8	22.7	25.0	PET
Cl Kα	19.2	26.8	30.2	PET
K Kα	27.0	43.0	53.3	PET

In general, count rates increase as the accelerating voltage increases, but the rate of increase is uneven among elements (Table I). The rate actually decreases at higher voltages for Na, due to heavy absorption of the relatively long wavelength Na K_α X-rays

by the aragonite matrix, even though the excitation efficiency increases. We suspect that this heavy absorption is due to pitting of the target surface, which often occurs at high voltages. In contrast, K K_α count rates increase substantially between 10 and 20 kV. This increase results from a large increase in the generation efficiency of this line at higher voltages and relatively little absorption of the emitted X-rays, which have the shortest wavelength of any element in our analyses. Correction factors for K, due to absorption, as computed for an aragonite matrix based on Philibert's formula (Philibert, 1963), are slight at all voltages tested; even at 20 kV, 95% of the X-ray intensities generated are counted. In contrast, for Na correction factors vary from 0.70 at 10 kV to only 0.39 at 20 kV, i.e., at voltages > 10 kV, the K_α count rates measured are only $\approx 1/2$ of the X-ray intensities actually generated.

Procedures for collecting data and correcting them for matrix effects at each voltage are illustrated in Table II. The comparison is based on count rates from parallel analyses with each accelerating voltage in the same area of the same otolith. The peak and background are measured in turn for each line, a subtraction is performed, and concentrations (computed weight-fractions, in p.p.m.) are calculated from the matrix corrections for aragonite. Measurement errors are estimated from Eqn. 1 and the detection limits are calculated by Ancey et al.'s (1978) method.

Two points are evident from Table II. First, background-corrected count rates show the same trends across elements and voltages as was evident in Table I. But second, percent measurement errors do not necessarily increase as background-corrected peak count rates decrease (e.g., S K_α at 15 and 20 kV). The measurement error decreases in this instance because the error term depends on both peak and background count rates, and the latter is lower for S at 20 kV than 15 kV. The optimal accelerating voltage has to be decided by balancing across elements the effects of different voltages on the error terms associated with each element, e.g., percent errors are lowest for Na K_α at 10 kV, but lowest for K K_α at 20 kV.

(1B) EFFECTS OF ACCELERATING VOLTAGE ON VOLUME OF X-RAY GENERATION

Particularly for focused electron probes, the voltage chosen should ensure that the volume of the target from which X-rays are generated is small enough to achieve the spatial resolution (e.g., distance between adjacent points) required of the scan or experiment. However, the voltage should also be large enough to ensure that most of the X-rays produced are generated below the surface layer, minimizing effects of any contamination or irregularities in the surface (while also bearing in mind that with the three-dimensional structure of otoliths, increasing the depth of the generation volume also increases the number of increments over which the data are acquired). The lateral diameter of the generation volume is given approximately by:

$$L = 0.154 \frac{(E_o^{1.5} - E_c^{1.5})}{\rho}, \tag{3}$$

TABLE II

Count rates, counting errors and corrected concentrations for same morwong otolith target at 10, 15 and 20 kV. ND, not detected. In this experiment, beam was defocussed to 50 μm diameter to minimize damage to target. Total dwell time of beam on target at end of experiment was 12 min (4 min at each voltage). Peak and background counting times were 60 and 30 s, respectively. Errors are calculated with $\chi^2 = 3.841$ and detection limits with $\lambda = 13.0$.

Element and line	Count rates in Hz		
	10 kV 37.5 nA	15 kV 25.0 nA	20 kV 18.75 nA
Na Kα			
peak	69.7	56.6	36.7
bgnd	11.0	8.7	5.1
peak-bgnd	58.7	47.9	31.6
Computed weight fraction (ppm)	2880	3100	2970
abs and % errors	(±119, 4.1%)	(±139, 4.5%)	(±162, 5.5%)
Detection limit			
Sr Lα			
peak	69.1	71.7	65.6
bgnd	37.6	40.3	33.7
peak-bgnd	31.5	31.4	31.9
Computed weight fraction (ppm)	1960	1625	1700
abs and % errors	(±189, 9.6%)	(±162, 9.9%)	(±156, 9.1%)
Detection limit			
S Kα			
peak	5.5	8.0	6.1
bgnd	2.1	3.8	2.5
peak-bgnd	3.4	4.2	3.6
Computed weight fraction (ppm)	410	380	330
abs and % errors	(±95, 23%)	(±90, 24%)	(±77, 23%)
Detection limit			
Cl Kα			
peak	5.0	6.1	6.1
bgnd	4.0	4.9	5.6
peak-bgnd	1.0	1.2	0.5
Computed weight fraction (ppm)	110 ND	90 ND	30 ND
Detection limit	200	140	130
K Kα			
peak	16.3	28.5	32.7
bgnd	7.9	11.0	10.8
peak-bgnd	8.4	17.5	21.9
Computed weight fraction (ppm)	750	840	880
abs and % errors	(±128, 17%)	(±86, 10.2%)	(±75, 8.5%)
Detection limit			

where L is the diameter of the volume (in μm) from which 95% of the generated X-rays are emitted, E_o is the accelerating voltage (in KeV), E_c is the excitation energy for the X-ray line (in KeV) and ρ is the density of the target. This expression follows Reed (1975), although modified slightly based on Heinrich's (1981) suggested relationship between the width and depth of X-ray generation.

An estimate of the depth into the target from which X-rays are received by the detectors is given by Heinrich (1981):

$$D = 0.07\ (E_o^{1.65} - E_c^{1.65})\frac{f}{\rho}\ , \tag{4}$$

where D is the depth (in μm) from which 95% of X-rays are received by the detector, ρ, E_o and E_c are as in Eqn. 3, and f is the absorption correction factor.

It is evident from these equations that, for a given accelerating voltage, L is largest and D smallest for Na, since it has the lowest excitation energy, and L smallest and D deepest for K, as it has the highest excitation energy. Calculated generation diameters and penetration depths for these elements at the three accelerating voltages considered and assuming a conservative otolith density of 3 are given in Table III. These values set the maximum spatial resolution that can be achieved in a life history scan. In many cases, even these values are impractical since it is necessary to degrade the horizontal resolution, by defocussing the beam, to minimize specimen damage (see below). A defocused 10-μm beam at 15 kV, for example, would generate Na K_α X-rays from an actual disc $\approx 14\ \mu$m in diameter. Furthermore, as target density almost certainly varies throughout an otolith (and is usually <3), even these values must be treated as approximations only.

(2A) BEAM POWER DENSITY AND SPECIMEN DAMAGE

The kinetic energy of the electrons in an EPMA beam is dissipated as heat in the target. In otoliths, the temperature rises sufficiently to decompose some of the carbonate, causing pitting (Fig. 5) and a loss of measurement accuracy. The rate of chemical change depends on the beam power density (BPD), which we define as:

$$\text{BPD} = \frac{E_o \times I}{A}\ , \tag{5}$$

where E_o is the accelerating voltage, I is the beam current and A is the area over which the electron beam is spread. (In a focussed beam, the beam spread is Gaussian, whereas in the defocussed condition, the beam is nearly uniformly spread over the sampled area, with only a slight Gaussian roll-off at the margins.)

The effect of changing beam power density on count rates and stability were determined for Ca, Sr and Na through a series of experiments, in which each of the three

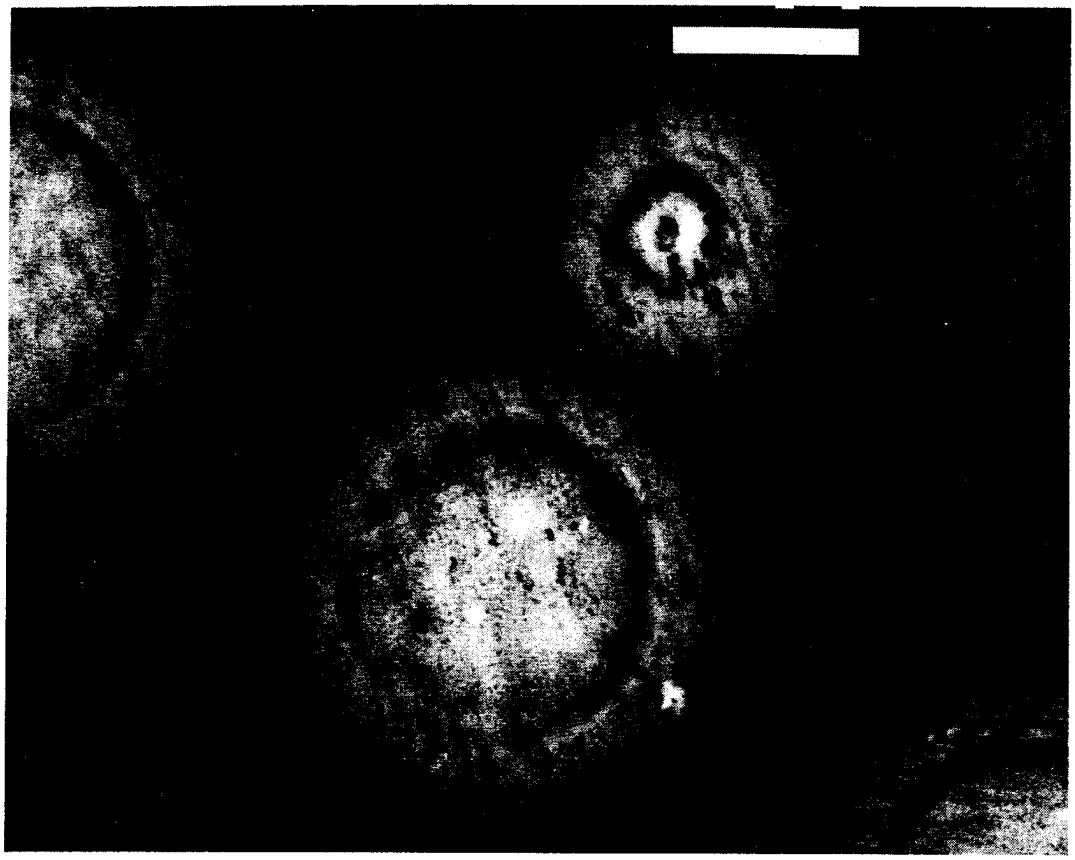

Fig. 5. Backscattered electron micrograph of target regions for two beam conditions on a *N. macropterus* sagitta. Uppermost target is for 14 μm diameter beam at 25 nA and 15 kV; smaller target is for a focussed (<5 μm diameter) beam of same power. Focussed beam produces a central bright region, indicative of extensive decomposition of $CaCO_3$, and severe pitting (black spots around and in target), which may be formed by escaping CO_2.

parameters that define beam power density (E_o, I and A) was varied independently. The number of counts in 5-s intervals were measured over periods of 120 s for Na and 240 s for Sr. Ca was measured on a second spectrometer at the same time as either the Na or Sr counts were being collected. Five replicates of each treatment were taken to estimate the variance in counts between different points in the same region of an otolith.

Experiment 1. The effects of spot size on count rates of Na K_α, Sr L_α and Ca K_α, voltage (15 kV) and beam current (25 nA) held constant; total dwell time 120 s.

Spot sizes ranged in diameter from a nominal 3 μm (focussed beam) to 20 μm (defocussed), which correspond to beam power densities ranging from nominally 50 to 1.2 $\mu W \cdot \mu m^{-2}$. The spot diameter was set by observing the cathodoluminescent disc through the optical microscope of the electron probe when it was targeted on a piece of polished thorium oxide. The effect of spot size on sodium, strontium and calcium counts in successive 5-s intervals is depicted in Fig. 6 and for Na and Sr normalized

TABLE III

Diameter (L) and depth (D) (in μm) of generation volume in aragonite from which 95% of X-rays emanate when beam is focused (after Reed, 1975; Heinrich, 1981).

Element and line	Accelerating voltage		
	10 kV, L/D	15 kV, L/D	20 kV, L/D
Na Kα	1.6/0.7	2.9/1.1	4.5/1.3
K Kα	1.3/0.8	2.7/1.8	4.3/2.9

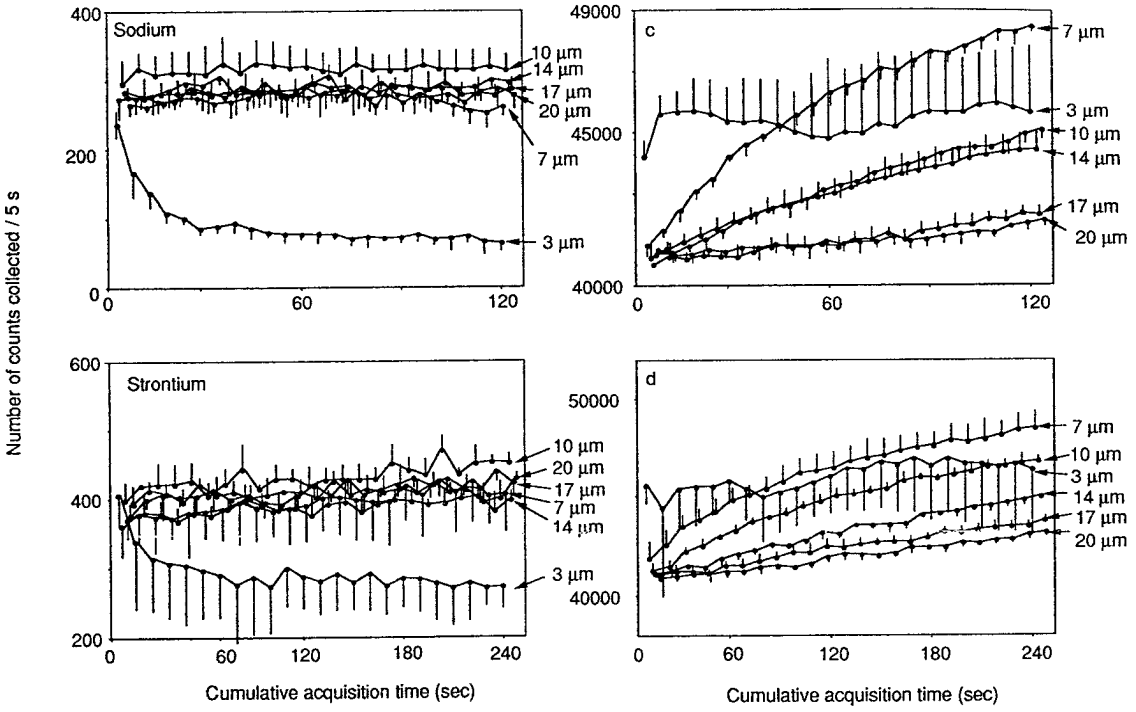

Fig. 6. Changes in counts for Na over 120 s total dwell time and Sr over 240 s total dwell time under constant beam power (accelerating voltage 15 kV, beam current 25 nA) and beam diameters ranging from 3 to 20 μm. (c) and (d) show corresponding changes in Ca counts. Each point is $\bar{x}$ and 1 SD of five replicate counts for each 5-s time interval.

to Ca in Fig. 7. The response patterns for Na, Sr and the normalized data are similar. For all but the 3- and 7-μm spots, counts are highly variable, but increase relatively stably over the 120 s. However, under a 3-μm beam, Na counts decreased rapidly to average -72.6% at the end of the full 120 s, most of this decline occurred in the first 30 s and Sr counts decline rapidly over the first 100 s. Calcium count rates also differed in pattern among treatments, increasing rapidly within the first 10 s of counting at 3 μm, increasing asymptotically at 7 and 10 μm and increasing linearly for the 17- and 20-μm treatments. The variance among replicate counts was extremely high at 3 μm (120% of the mean), but much less at other spot sizes. Results for Na : Ca and Sr : Ca ratios,

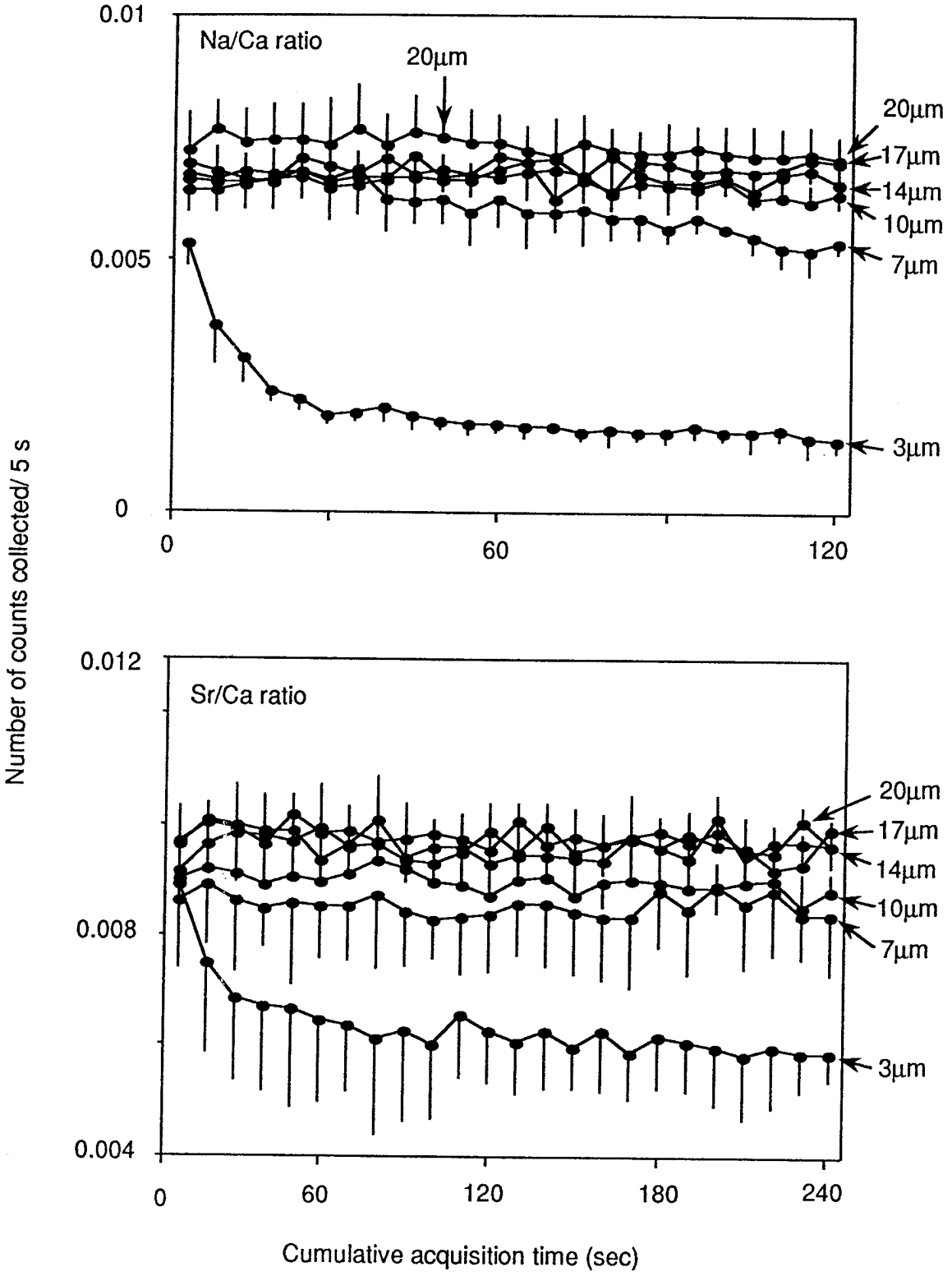

Fig. 7. Change in Na : Ca and Sr : Ca ratios over total dwell times of 120 and 240 s, respectively, under constant beam power (accelerating voltage 15 kV, beam current 25 nA) and beam diameters from 3 to 20 μm. Each point is $\bar{x}$ and 1 SD of five replicate counts for each 5-s time interval. For clarity, only one side of SD bar is shown.

in gener
behavior
The o
point (9.

Fig. 8.
over 12

in general, paralleled those for the elements without normalization, with the erratic behavior of Ca appearing to have little effect.

The overall change in Ca counts correlated with beam power density up to a certain point (9.7 $\mu W \cdot \mu m^{-2}$), above which the relationship appears to break down (Fig. 8).

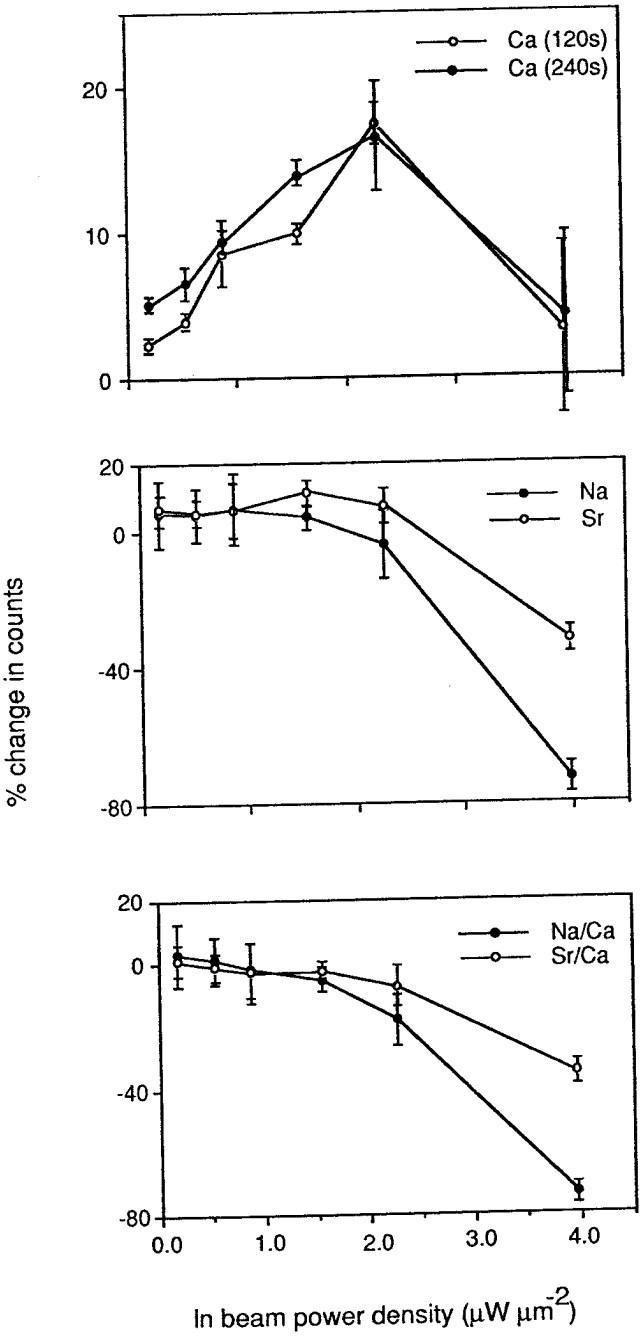

Fig. 8. Relationship between BPD and change in counts of Ca, Sr and Na and Sr : Ca and Na : Ca ratios over 120 and 240 s. Each point represents $\bar{x}$ (and 1 SD) change in counts between first counting period (after 5 s) and last (after either 120 or 240 s).

Changes in Na, Sr and normalized data are relatively unaffected by beam power densities $< \approx 2\,\mu W \cdot \mu m^{-2}$, but then increase (negatively) at higher values (Fig. 8).

Experiment 2. The effects of voltage on counts of Na K_α, Sr L_α and Ca K_α, beam diameter (14 μm) and current (25 nA) held constant; total dwell time 120 s.

The voltages tested ranged from 10 to 25 kV, corresponding to a range of beam power densities of 1.6–4.1 $\mu W \cdot \mu m^{-2}$. The results are depicted in Fig. 9. At the three lower voltages tested, Na and Ca counts and the Na : Ca ratio increased slightly with dwell time. However, changes in Na counts and the Na : Ca ratio are negative at 25 kV, whereas Ca count rates continued to increase.

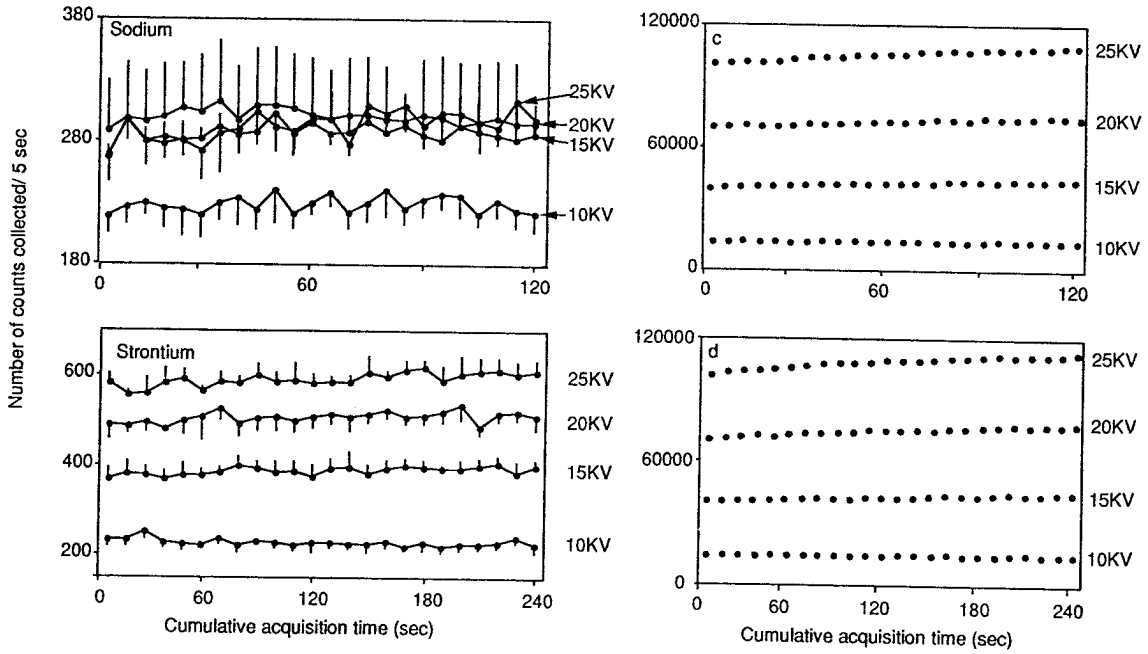

Fig. 9. Change in Na and Sr counts over total dwell times of 120 and 240 s, respectively, under constant beam diameter (14 μm), constant beam current (25 nA) and accelerating voltages from 10 to 25 kV. (c) and (d) shown corresponding counts for Ca. Each point is $\bar{x}$ and 1 SD of five replicate counts for each 5-s time interval. For clarity, only one side of SD bar is shown.

Changes in Sr counts (Fig. 9) were smaller than those in Experiment 1. Except for the 10-kV treatment, for which Sr counts decreased over the 240 s, all voltages tested resulted in small, linear increases in Sr counts. Calcium counts were stable at 10 kV, but increased asymptotically at other voltages (net mean increases of + 9.4, + 10.1 and + 10.4% for 15, 20 and 25 kV, respectively). Changes in Sr : Ca ratios over 240 s were small and negative.

Experiment 3. The effects of beam current on counts of Na K_α, Sr L_α and Ca K_α, beam diameter (14 μm) and voltage (15 kV) held constant; counting time 120 s.

Beam currents ranged from 10 to 40 nA, corresponding to beam power densities of 1–3.9 $\mu W \cdot \mu m^{-2}$. The results are depicted in Fig. 10. Na counts changed little over the total 120 s dwell time, but in all cases changes were positive. Ca counts also increased in all treatments; the extent of the change correlated with the beam power density. Na : Ca ratios increased slightly in the 10-nA treatment, but decreased slightly at 25 and 40 nA.

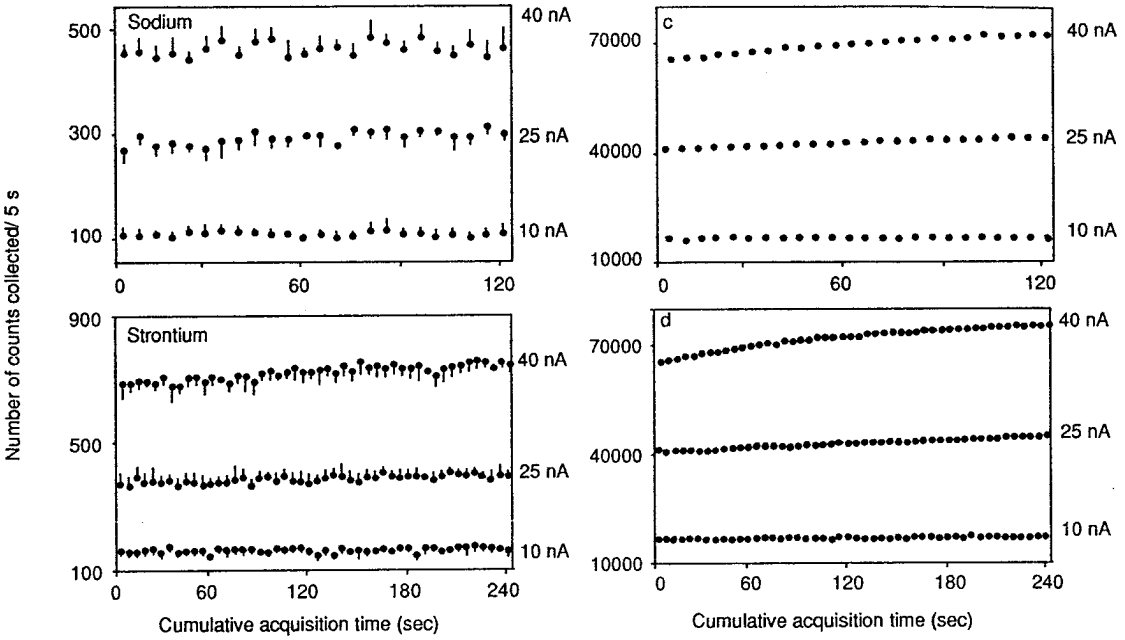

Fig. 10. Change in Na and Sr counts over total dwell times of 120 and 240 s, respectively, under constant beam diameter (14 μm), constant accelerating voltage (15 kV) and beam currents from 10 to 40 nA. (c) and (d) show corresponding counts for Ca. Each point is $\bar{x}$ and 1 SD of five replicate counts for each 5-s time interval. For clarity, only one side of SD bar is shown.

Mean Sr counts changed minimally at 10 nA, but increased 6.8 and 8.8% at 25 and 40 nA, respectively (Fig. 10). In general, the higher the beam current, the greater the variance in Sr counts. Ca counts increased with time in all three treatments, the extent of change being proportional to the beam power density. Sr : Ca ratios decreased slightly over the 240 s in all treatments.

SUMMARY AND INTERPRETATION OF EXPERIMENTAL RESULTS

The results of these experiments document that variations in any of the three beam operating parameters (spot size, voltage and current) can change the count rates of the elements that constitute an otolith's aragonite-protein matrix. The nature, direction and magnitude of these changes were not simple, but rather appear to reflect the influence of several different factors. First, in many tests, count rates increase with time, either abruptly or as long term linear or asymptotic trends. Such an increase, evident in Ca

K_α, Sr L_α and Na K_α, occur when the weight fraction of an element increases due to decomposition of the carbonate and subsequent loss of the target's mass. In all three elements, however, the positive trend eventually breaks down and counts decline markedly (Fig. 8). At high beam power densities (such as when using the focussed beam), this decline begins almost immediately during acquisition (Fig. 6).

We attribute these declines to the effects of pitting. When a pit appears in the surface of an otolith, the emitted X-rays are heavily absorbed, due to an increased path length. All elements are affected by this process, though the magnitude of the effect differs between elements, corresponding to the energy of their respective X-rays (i.e., because Ca K_α X-rays are more energetic than those of Sr L_α and Na K_α there is less absorption and less attenuation until pitting is severe). It is difficult to determine when in an analysis the effects of pitting outweigh any effects of chemical change on count rates. In the 25-kV treatment in Experiment 2, for example, Na counts increased over the first 90 s only to fall during the final 30 s. Presumably, after 90 s the effects of pitting outweighed those of chemical change. The difficulty lies in measuring the effect of pitting 10, 30 or 60 s into the analysis. Since the absorption coefficient for Na K_α in $CaCO_3$ is very similar to that in CaO, the Na K_α count rate should change at a rate similar to Ca K_α, if pitting was not a factor. In fact, this was not the case in our experiments: when Na counts increased, they did so more slowly than Ca counts. Sr counts also fell – presumably due to pitting – when small spot sizes and high beam power densities were used. We conclude, therefore, that pitting is always a factor when otoliths are analysed with WD EPMA and always affects perceived X-ray count rates.

(3) SELECTION OF COUNTING TIMES AND SCHEDULING OF SPECTROMETERS

As with all of the other parameters that need to be considered in formulating a set of operating conditions, the choice of suitable counting times is a compromise between the accuracy and precision desired and the time available to analyse the required number of points. Elements for which peak-to-background ratios are high (e.g., Ca) generally require shorter counting times than those for which the ratio is low (e.g., Cl or S). The counting times we used in routine analysis of the six elements (other than carbon and oxygen) most abundant in otoliths (Ca, Na, Sr, K, S and Cl) are given in Table IV. These acquisition times were chosen in part on the basis of our pilot studies and in part on indications from the literature of the degree to which the concentrations of these elements vary in otoliths. The time spent in moving spectrometers and doing matrix corrections on-line is $\approx 13\%$ of counting time.

In scans where several elements are to be analysed at each point, scheduling of the serial measurements of the spectrometers depends on the relative stability of the count rates and the precision required for each element. Table IV shows one of our typical schedules. To save machine time, backgrounds were measured on only one side of each peak and extrapolated to the position of the peak with a measured gradient. Each scan point took 4 min. The elements that are normally found in lowest concentrations share

TABLE IV

Typical scheduling of three WD spectrometers to measure six elements (time taken to complete each count is given in brackets).

Spectrometer Crystal	3 TAP	2 PET	1 PET
	Na K_α pk (60 s), background (30 s)	K K_α pk (60 s), background (30 s)	S K_α pk (60 s), background (30 s)
	Sr L_α pk (60 s), background (30 s)	Ca K_α pk (10 s), background (5 s)	Cl K_α pk (60 s), background (30 s)
	On-line PAP matrix correction		(12 s)
	Beam current measurement		(10 s)
	Spectrometer movement		(20 s)

Spectrometer 1. For this spectrometer, we calculated the trade-off between counting times and measurement precision for K and Cl, and chose a time allocation that gave us the best combination. Ca is measured about half way through the analysis, because all elements are to be normalized to it. On Spectrometer 3, sodium was measured before strontium because Na K_α counts are more likely to be severely affected by pitting.

(4) STANDARDS AND CORRECTION FOR SPECTROMETER DRIFT

When unknown materials are analysed with EPMA, standards are routinely measured in parallel to check for spectrometer drift (e.g., slight changes in the position of the analysing crystal resulting from changes in, for example, temperature) during extended runs. The standards used in our studies are given in Table V. Throughout our studies, Ca, Sr and S standards were measured at the beginning and end of each life history scan, as well as at every 60 points throughout "long" scans. Spectrometer drift was generally very slight, in the order of 1–3%, but very occasionally, drift resulted in

TABLE V

Standards used in WD life-history scans of otoliths.

Element	Line	Standard	
Ca	K_α	Wollastonite	$CaSiO_3$
Sr	L_α		$SrTiO_3$
S	K_α	Pyrite	FeS_2
Na	K_α	Jadeite	$NaAlSi_2O_6$
K	K_α	Adularia	$KAlSi_3O_8$
Cl	K_α		AgCl

Na, K and Cl standards are unstable under a dwelling point beam, so standard count rates must be acquired with a 50-μm moving beam. As standards for Ca, Sr and S are stable, these are used to check for spectrometer drift during scanning.

differences of up to 15% between initial and final standard counts. The reasons for these extreme cases are not known. However, there was some indication that spectrometer drift was highest when room temperatures or atmospheric pressure varied significantly during a scan.

We corrected for spectrometer drift by multiplying estimated weight fraction concentrations by correction coefficients calculated by linear interpolation between the initial and final measurements of the standards. This procedure obviously assumes drift is

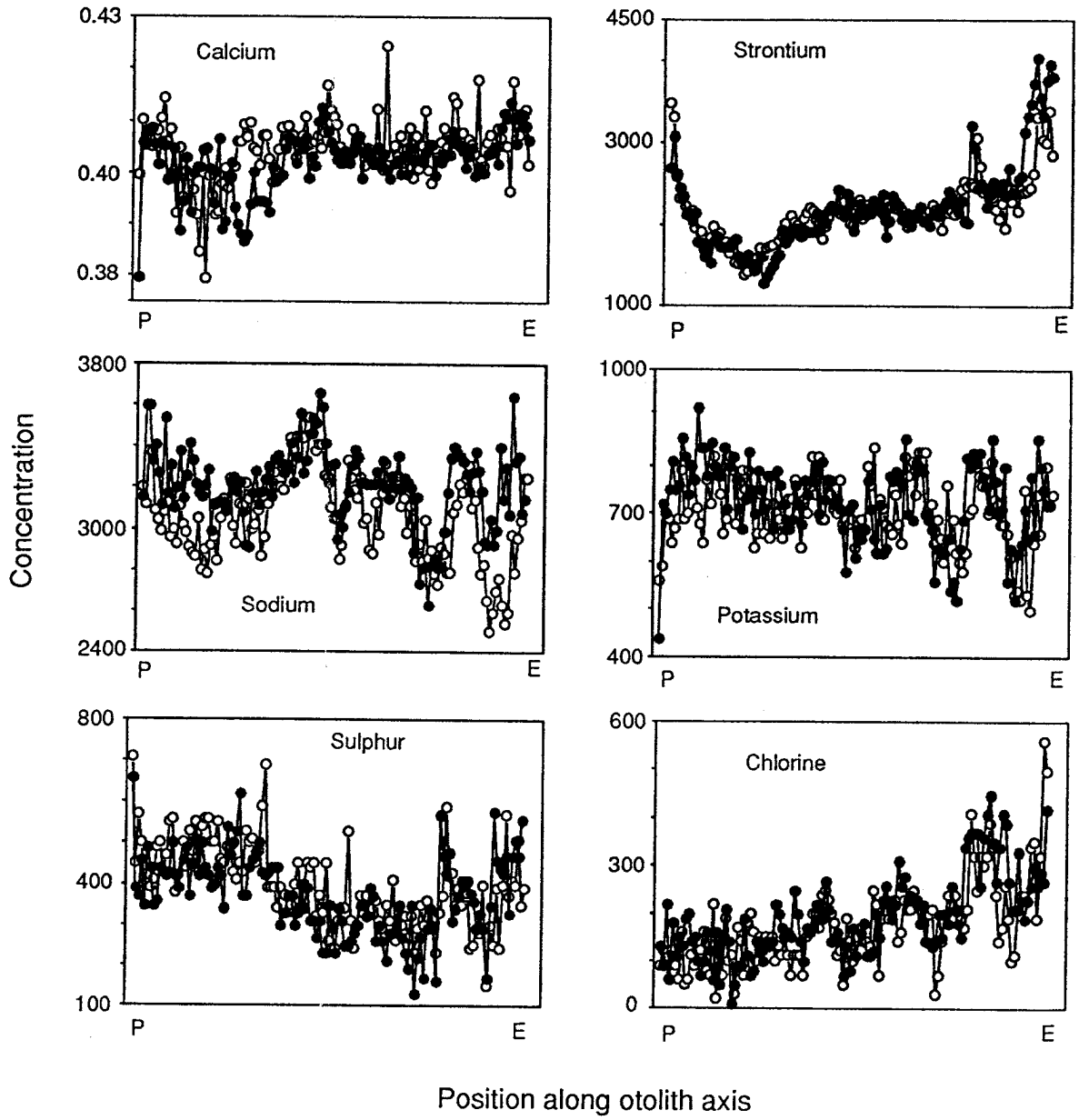

Fig. 11. Raw data from life-history scans for left (open circle) and right (solid circle) sagitta of a *N. macropterus*. Beam power density was 2.4 $\mu W \cdot \mu m^{-2}$, beam diameter 14 μm and spacing between points 25 μm. P, primordium, E, edge of otolith.

TABLE VI

Minimum detection limits, amount of measurement error and $\bar{x}$ and ranges of estimated concentrations (weight fractions), for *N. macropterus* and *T. maccoyii*, of six elements that can be assayed reliably with a WD electron probe. Values for *N. macropterus* and *T. maccoyii* are based on a random subset of our data, include numerous individuals and positions along scanned axis of points analysed in two species. Values illustrate concentrations in two species; they are not definitive means and ranges. n = 478 points for *N. macropterus* and 120 points for *T. maccoyii*. Concentrations are given in ppm, except for Ca which is in percent of target mass. Note that values below minimum detection limit are effectively 0.

Element	Minimum detection limit	*N. macropterus*		*T. maccoyii*	
		Mean (range) concentration	Measurement error (absolute, %)	Mean (range) concentration	Measurement error (absolute, %)
Ca	–	38.8% (35.3–44.5)	–	40.6% (39.2–41.2)	–
Sr	311	2240 (1430–3860)	±157 (7%)	1626 (1070–2380)	±153 (9%)
Na	159	3331 (2680–4240)	±122 (3.7%)	2916 (1590–3790)	±117 (4%)
K	136	729 (280–1630)	±72 (10%)	442 (230–750)	±67 (15%)
S	149	421 (220–1220)	±76 (18%)	392 (210–790)	±75 (19%)
Cl	157	255 (0–1230)	±72 (28%)	272 (10–1170)	±72 (26%)

linear, but this assumption can be tested at any stage of an analysis if it is in doubt. We also arbitrarily discarded life-history scans in which spectrometer drift exceeded 5% for any one of the three standards.

Experimental Test of Measurement Error

The ultimate tests of the procedures developed above are to determine, first, the extent to which they produce consistent estimates of concentrations and, second, whether patterns in the variation of these concentrations can be consistently replicated within and between specimens. In practical terms we undertook these tests by measuring the degree to which parallel life-history scans in two otoliths from the same fish indicated similar ontogenetic variation in element concentrations. Assuming that the chemistry of otolith deposition does not differ between the two sides of the endolymphatic system, otoliths from the same animal should have identical chemical patterns. Hence, differences between the two life-history scans would reflect the limits of our procedures, that is, specifically, the combined effects of the quality of specimen preparation (including the extent to which we could section along the same growth axis in the two otoliths), of the beam power settings we used and of inherent measurement error. The comparison indicates the limits to which EPMA of elemental variations can be used for assessing biological significance, under our operating conditions.

The comparisons were done with pairs of sagittae from *N. macropterus*. A number of comparisons were done; the results from all were similar and those from one chosen at random are depicted in Fig. 11. Plots for each element for the two otoliths overlapped closely and, in all elements, indicated similar patterns of ontogenetic variation. Aside from occasional single point "spikes", the estimated absolute concentrations were virtually identical in the two otoliths for all elements except sodium. For sodium, both ontogenetic patterning and mean absolute concentrations were much the same in the two otoliths, but for reasons not yet clear to us the tracks diverged slightly in this individual near the primordium and edge. Interestingly, K and S also show evidence albeit much less than for Na at about the same positions, which may indicate differences between the otoliths in their growth characteristics. However, such divergence was not typical in our left/right comparisons, and in general, we conclude that our methods produce a high level of repeatability in both the patterning and absolute concentrations of all six elements assayed.

Discussion

There are clear differences between the abilities of ED- and WD-based EPMA to detect and accurately quantify the elements in the calcium carbonate matrix of an otolith. The conventional ED electron probe is severely limited in its ability to detect elements present in concentrations < 1000 ppm because of difficulties in resolving line overlaps, the presence of spectral artifacts and the generally low peak-to-background ratios and low peak count rates. Nonetheless, some improvements in using these

spectrometers for life-history scanning may be possible. Systematic errors, for instance, can sometimes be avoided by compromising on other analytical parameters. For example, when the background is linear and there are no interfering lines or artifacts, Sr could be measured on an ED system using the Sr K_α line at 14.14 kV. However, the accelerating voltage would have to be increased to 35 kV to obtain sufficient excitation efficiency, which may be undesirable because the primary electrons are scattered through a large volume and correction procedures for the other, lighter elements become unreliable. Systematic errors in the measurement of Na K_α could also be reduced if a thin window or windowless detector were used; these detect Na K_α X-rays more efficiently and produce a flatter background spectrum at this line energy than the conventional Be window detector we used. The minimum detection limits for lines near large peaks (e.g., K K_α) might also fall due to the impressive gain in energy resolution (< 130 eV for Mn K_α) recently achieved by ED manufacturers, largely without sacrificing counting speed. The new thin-window germanium detector for the soft X-rays used in microprobe analysis avoids the problem of the escape peak overlapping Sr L_α, although it does create a new overlap between the Ge L_α and Na K_α lines. However, the energy resolution is high (≈ 135 eV for Mn K_α) and this type of detector shows promise for studies of "age determination", in which Sr is the primary element of interest (e.g., Radtke & Targett, 1984). Given these recent advances in ED spectrometers, and the fact that they are cheaper and more widely available than WD systems, we are continuing our work on defining the areas of life-history scanning that might be amenable to ED spectrometry.

Until the difficulties in conventional ED-based EPMA can be resolved, we suggest such systems be used cautiously for detecting and measuring trace elements in otoliths, particularly if many elements are likely to be present. In a recent study using an ED spectrometer, Mulligan et al. (1987) determined the presence or absence of 34 trace elements in the otoliths of striped bass *Morone saxatilis* from tributaries of Chesapeake Bay, USA. They did not report the concentrations detected, but it seems likely from our research that, other than carbon and oxygen, only three elements – Ca, Sr and Na – routinely occur in concentrations of > 500 ppm. Unless the otoliths of *M. saxatilis* differ markedly from those we have examined, Mulligan et al. (1987) detected elements at concentrations of < 0.1 wt (1000 ppm), which is the practical minimum detection limit of an ED spectrometer [for some elements, the limit can be as high as one or two percent when lines overlap broadly (Statham, 1981)]. It is not clear how Mulligan et al. (1987) achieved the sensitivity they reported.

Unfortunately, Mulligan et al. (1987) also give no indication of their criteria of detection, although calculating the minimum detection limit at a given confidence level must precede detection. Ancey et al. (1978) showed that the minimum detectable concentration $C_{\min}$ is given by:

$$C_{\min} = \frac{FC_s}{I}\left[\frac{\lambda}{2t}\left(1 + \sqrt{1 + \frac{4Bt(1 + a^{-1})}{\lambda}}\right)\right], \qquad (6)$$

where C_s is the concentration of the element in the standard, F is a matrix correction factor, which corrects for effects of absorption, electron backscattering and fluorescence in both standard and unknown, I is the peak count rate on the standard for the line being measured, B is the background count rate on the unknown (in this case the otolith), t is the peak counting time on the unknown, λ determines the level of confidence (e.g., it is 13 for a 5% risk of both kinds – that of detecting the element when it is, in fact, not present and also of not detecting it when it is, in fact, present), and a is the ratio of the background to peak counting times (for ED spectrometers, $a = 1$). Any concentration "measured" less than C_{min} is meaningless and the element has not been detected. For purposes of statistical analysis, we record as zero any "measured" concentration less than the minimum detection limit. It is not clear how Mulligan et al. (1987) treat values less than C_{min}. This is particularly worrying in that they report the presence in otoliths of such elements as technetium (Tc), which is a radioactive element produced in fission reactors and released into the environment in minute quantities from medical laboratories. It is likely that the reported "detection" of Tc is due to an inadequate definition of detectability rather than extraordinarily high levels of the element in the environment.

Mulligan et al. (1987) also reported detecting the rare earth elements (REEs) Ce, Pr, Sm, Gd, Tb, Dy, Ho, Er, Tm and Yb in *M. saxatilis* otoliths. The L spectrum of these elements, which is used to assay their presence, contains at least 10 lines with intensities of $> 1\%$ of the respective L_α line. Because the L_α lines for all of these elements lie between 4 and 11 keV, overlaps are numerous (even for WD spectrometers), making their individual detection and measurement virtually impossible at low concentrations. With ED spectrometers, the overlaps are particularly severe for atomic number differences between 2 and 5 (Smith & Reed, 1981). Errors in measuring the lighter REEs affect measurements of the less abundant heavier ones (Haskin & Paster, 1984) through the use of overlap coefficients. The heavier, odd-numbered REEs have been measured with a WD spectrometer (Amli, 1975), but only at concentrations of ≈ 3000 ppm by weight and only in mineral phases where the lighter REEs are virtually absent. Therefore, Mulligan et al.'s (1987) report of detecting Ho and Tm by ED-based EPMA appears incredible, unless these elements have been bio-concentrated to an extraordinary degree in otoliths.

Finally, it should be noted that extensive line overlaps are not confined to the rare earth elements; K_α and K_β lines overlap extensively between neighbors for elements with atomic numbers 22–30 (Ti to Zn). Pulse pile-up and silicon escape peaks add to the interference problem. Given such difficulties, it is essential that studies such as Mulligan et al.'s (1987) report not only statistical criteria for detection, but also techniques for dealing with line overlaps and spectral artifacts. Without such details, other workers cannot assess the accuracy of the nominally effective stock discrimination of *M. saxatilis* reported by Mulligan et al. (1987).

In summary, at counting times of > 10 min, ED spectrometers can detect concentrations of elements within otolith aragonite matrices as low as ≈ 500 ppm, but only if

artifacts, overlaps and nonlinearities in the background can be accurately modelled. This will not generally be the case and especially not when large numbers of elements are being assessed. We conclude that the ED spectrometer is not generally effective for measuring trace element levels and for scanning life-histories in otoliths. Whether they are adequate for measuring concentrations in other calcified structures in fishes, e.g., scales and vertebrae (see, e.g., Sauer & Watabe, 1989), remains to be determined.

OPERATING PARAMETERS AND DATA QUALITY IN WD-BASED EPMA

WD-based EPMA is nominally capable of detecting and accurately measuring elements present at concentrations of > 100 ppm. In the otoliths we have examined, this effectively limits the elements to six: Ca, Na, Sr, K, S and Cl. Carbon and oxygen, which are also abundant in aragonite matrices, can be measured with a WD microprobe but the concentrations of both are very unstable under the electron beam and hence they are not routinely analysed. We have rarely found other elements, such as Mg, Fe and Zn, in concentrations of > 100 ppm. We note, however, that our samples include only a limited number of species (albeit ecologically quite diverse), and that further work on additional species is clearly needed before broad generalizations about element concentrations in otoliths are warranted.

The effect of the electron beam on the otolith must be considered in interpreting data produced by a WD system. Our tests indicate that the extent and nature of the damage incurred, and hence the quality of the data, are closely related to the beam power used in the analysis and the area over which the electron beam is spread, that is, beam power density. The greater the beam power density, the greater the damage and the lower the data quality, but the faster the acquisition rate. As machine time is expensive, individual operators will always have to decide how much damage is acceptable. At the other extreme, very low beam power densities ensure minimal chemical change and pitting, but also require very long counting times to provide viable measurements for elements that are present at low concentrations. Unless very accurate estimates are required, machine time is unlimited or very few points are to be analysed, beam power densities $< \approx 0.5\ \mu W \cdot \mu m^{-2}$ seem to us to be rarely warranted.

We settled upon a maximum beam power density of $3\ \mu W \cdot \mu m^{-2}$ as an acceptable compromise between damage and acquisition rate. At densities below this, count rates of Ca, Sr and Na counts are relatively stable and the normalized Sr : Ca and Na : Ca ratios decline only slightly with increasing dwell time (up to the limits required to acquire enough counts for measurement errors to be $< \approx 5\%$). In practice, of course, the time taken to analyse each point depends upon the desired degree of accuracy and the number of elements sought, both of which depend on levels of natural variability and on the objectives of the study.

Because of the very high beam power densities focussed beams ($\leqslant \approx 5\ \mu m$ diameter) entail, even if scanned, they do not, in our experience, produce adequate stability within an otolith matrix for effective measurement of concentrations of most elements. In

addition to producing chemical change and pitting, focussed beams also often disrupt the surface coating, with resultant charging of the target. Not only does damage of this kind result in erroneous estimates, but also – and perhaps more importantly – the extent of this error is difficult to quantify. Unless one is prepared to accept (or ignore) such sources of systematic error, focussed beams do not appear suitable for the analysis of otoliths. Parenthetically, scanning the beam without defocussing does not appear to be an effective means of reducing damage. The heating from a focussed beam scanned once over a given area has a greater, and less predictable, effect on data quality than that from a beam defocussed to cover that same area.

Assuming one operates at a fixed "safe" beam power density and noting that the counting error is inversely proportional to the square root of the number of counts collected, then it follows from Eqns. 2 and 5 that this counting error (E) is related to the beam diameter (d) and the counting time (t) by the proportionality:

$$E \propto \frac{1}{d\sqrt{t}} . \tag{7}$$

That is, counting errors decline rapidly with an increase in beam diameter, but much more slowly as counting time increases. As increasing beam diameter also permits an increase in the beam power without changing the damage rates, it follows that whenever possible the beam diameter should always be set to the highest possible value, that is, the largest consistent with the spatial resolution required by a particular study. Adjacent points in an analysis, however, still need to be separated by at least 4 μm, because of beam spreading in the target.

MEASUREMENT ERROR AND SCALES OF NATURAL VARIABILITY IN OTOLITHS

The aim of any measurement procedure is to reduce measurement error to levels less than the signal being sought. Obviously, the greater the signal-to-error ratio the more confidence one has in the measurement. Assuming that the effects of beam damage, pitting and the like have been taken into account, the resulting measurement error in analysing otoliths has two very different components: that due to counting statistics and that due to inherent, small-scale variability in the otolith's composition. The first component can be readily quantified by standard analyses, and are summarized in Table VI. Given the count rates we can achieve without undue specimen damage, our estimates of composition range in accuracy from $\approx 4\%$ for Na to $\approx 20\%$ for S and Cl. Not surprisingly, the more abundant the element in an otolith, the better the counting statistics and the more accurate our estimates. Hence, at the concentrations we routinely measure and on the basis of machine properties alone, differences between points or individuals in Na concentrations of $< \approx 5\%$ and in Cl levels of $< \approx 20\%$ are noise. Determining the magnitude of measurement error induced by microscale differences in composition, which is below the scale involved in our life-history scans, is more difficult.

Parallel runs on pairs of otoliths (Fig. 11) suggest that error due to this scale of natural variability is of the same order of magnitude as that due to statistical properties of count rate acquisition. We have found that filtering the raw data with a 5 point moving average eliminates much of this noise while still retaining what appears to be the biologically significant signal in the data. We emphasize, however, that this is a wholly subjective and arbitrary decision until the scale of the relevant signal can be determined from suitably designed field and laboratory studies.

For the six elements that we routinely assay, the counting error, approximate sampling error and scale of natural variability of concentrations for the two species of fish with which we have worked extensively are given in Table VI. In all instances, the scale of natural variability in both species exceeded by at least an order of magnitude the combined counting and sampling measurement errors. On that basis, we conclude that our procedures are adequate and sufficient for determining at least the major ontogenetic trends in the deposition of these macroconstituents in the otolith and for using such data in studies of stock discrimination and population structure.

ACKNOWLEDGEMENTS

We thank T. Carter, A. Gronell and A. Jordan for assistance in laboratory and field studies, J. Kalish, N. Manning and T. Rees for advice on specimen preparation, V. Mawson, P. Miller and S. Sie for comments on the manuscript, and C. McRae and P. Rummel for assistance in microprobe analysis and discussion of results. We also thank the two journal referees (one anonymous, one not) for their useful comments on the ms. This study was funded in part by grants 1987/15 and 1989/30 from the Australian Fishing Industry Research and Development Committee.

REFERENCES

Amli, R., 1975. Mineralogy and rare earth geochemistry of apatite and xenotime from the Gloserheia granite pegmatite, Froland, Southern Norway. Am. Mineral., Vol. 60, pp. 607–620.

Ancey, M., F. Bastenaire & R. Tixier, 1978. Applications of statistical methods in microanalysis. In, *Microanalysis and scanning electron microscopy*, edited by F. Maurice et al., *Proc. Summer School St. Martin-d'Heres, 1978*, Les Editions de Physique, Orsay, France, pp. 319–343.

Bagenal, T.B., F.J.H. Mackereth & J. Heron, 1973. The distinction between brown trout and sea trout by the strontium content of their scales. *J. Fish Biol.*, Vol. 5, pp. 555–557.

Behrens Yamada, S., T.J. Mulligan & D. Fournier, 1987. Role of environment and stock on the elemental composition of sockeye salmon (*Oncorhynchus nerka*) vertebrae. *Can. J. Fish. Aquat. Sci.*, Vol. 44, pp. 1206–1212.

Bennett, J.T., G.W. Boehlert & K.K. Turekian, 1982. Confirmation of the longevity in *Sebastes diploproa* (Pisces: Scorpaenidae) from $^{210}Pb/^{226}Ra$ measurements in otoliths. *Mar. Biol.*, Vol. 71, pp. 209–215.

Buchardt, B. & P. Fritz, 1978. Strontium uptake in shell aragonite from the freshwater gastropod *Limnaea stagnalis*. *Science*, Vol. 199, pp. 291–292.

Calaprice, J.R., 1971. X-ray spectrometric and multivariate analyses of sockeye salmon (*Oncorhynchus nerka*) from different regions. *J. Fish. Res. Bd Can.*, Vol. 28, pp. 369–377.

Calaprice, J.R., 1983. X-ray fluorescence study of stock variation in bluefin tuna. Status report submitted to NMFS, Miami, March 1983, 60 pp.

Calaprice, J.R., 1985. Chemical variability and stock variation in northern Atlantic bluefin tuna. *Collect. Vol. Sci. Pap. ICCAT/Recl. Doc. Sci. CICTA/Collecc. Doc. Cient. CICAA.* Vol. 24, pp. 222–254.

Calaprice, J.R., L.A. Lapi & L.J. Carlsen, 1975. Stock identification using X-ray spectrometry and multivariate techniques. *Bull. INPFC*, Vol. 32, pp. 81–101.

Calaprice, J.R., H.M. McSheffrey & L.A. Lapi, 1971. Radioisotope X-ray fluorescence spectrometry in aquatic biology: a review. *J. Fish. Res. Bd Can.*, Vol. 28, pp. 1583–1594.

Campana, S.E., K.C.T. Zwanenburg & J.N. Smith, 1990. $^{210}Pb/^{226}Ra$ determination of longevity in redfish. *Can. J. Fish. Aquat. Sci.*, Vol. 47, pp. 163–165.

Carlstrom, D., 1963. A crystallographic study of vertebrate otoliths. *Biol. Bull.*, Vol. 125, pp. 441–463.

Degens, E.T., W.G. Deuser & R.L. Haedrich, 1969. Molecular structure and composition of fish otoliths. *Mar. Biol.*, Vol. 2, pp. 105–113.

Devereaux, I., 1967. Temperature measurements from oxygen isotope ratios of fish otoliths. *Science*, Vol. 155, pp. 1684–1685.

Edmunds, J.S., M.J. Moran & N. Caputi, 1989. Trace element analysis of fish sagittae as an aid to stock identification: pink snapper (*Chrysophrys auratus*) in Western Australian waters. *Can. J. Fish. Aquat. Sci.*, Vol. 46, pp. 50–54.

Fisheries Agency of Japan, 1967. Study on identification of the Pacific salmon by neutron activation analysis. Survey and Research Division, Fisheries Agency of Japan. [Cited in Mulligan et al. (1983)].

Gauldie, R.W., D.A. Fournier, D.E. Dunlop & G. Coote, 1986. Atomic emission and proton microprobe studies of the ion content of otoliths of chinook salmon aimed at recovering the temperature life history of individuals. *Comp. Biochem. Physiol. A*, Vol. 84, pp. 607–615.

Gauldie, R.W., E.J. Graynoth & J. Illingworth, 1980. The relationship of the iron content of some fish otoliths to temperature. *Comp. Biochem. Physiol. A*, Vol. 66, pp. 19–24.

Gauldie, R.W. & A. Nathan, 1977. Iron content of the otoliths of tarakihi (Teleostei : Cheilodactylidae). *N.Z. J. Mar. Freshwater Res.*, Vol. 11, pp. 179–191.

Goldstein, J.I., D.E. Newbury, P. Echlin, D.C. Joy, C. Fiori & E. Lifshin, 1981. *Scanning electron microscopy and X-ray microanalysis.* Plenum Press, New York, 673 pp.

Haskin, L.A. & T.P. Paster, 1984. Geochemistry and mineralogy of the rare earths. In, *Handbook of physics and chemistry of the rare earths. Vol. 3*, edited by K.A. Gschneider Jr. & L. Eyring, North-Holland Physics Publishing, Amsterdam.

Heinrich, K.F.J., 1981. *Electron beam X-ray microanalysis.* Van Nostrand Reinhold, New York, pp. 418–421.

Houck, J.E., R.W. Buddemeier, S.V. Smith & P.J. Jokiel, 1977. The response of coral growth and skeletal strontium to light intensity and water temperature. In, *Proc. Third Int. Coral Reef Symp. Miami, Vol. 2*, edited by D.L. Taylor, pp. 425–431.

Johnson, M.G., 1989. Metals in fish scales collected in Lake Opeongo, Canada, from 1939 to 1979. *Trans. Am. Fish. Soc.*, Vol. 118, pp. 331–335.

Kalish, J.M., 1989. Otolith microchemistry: validation of the effects of physiology, age and environment on otolith composition. *J. Exp. Mar. Biol. Ecol.*, Vol. 132, pp. 151–178.

Karakiri, M. & H. von Westernhagen, 1988. Apparatus for grinding otoliths of larval and juvenile fish for microstructure analysis. *Mar. Ecol. Prog. Ser.*, Vol. 49, pp. 195–198.

Klokov, V.K. & L.A. Frolenko, 1970. Elementary chemical composition of scales of pink salmon. *Izv. Tikhookean. Nauchno-Issled. Instit. Rybn. Khoz. Okeanogr.*, Vol. 71, pp. 159–168.

Lapi, L.A. & T.J. Mulligan, 1981. Salmon stock identification using a microanalytic technique to measure elements present in the freshwater growth region of scales. *Can. J. Fish. Aquat. Sci.*, Vol. 38, pp. 744–751.

Morales-Nin, B., 1987. Chemical composition of the otoliths of the sea bass (*Diacentrarchus labrax*) (Linnaeus, 1758) (Pisces, Serranidae). *Cybium*, Vol. 10, pp. 115–120.

Moreton, R.B., 1981. Electron-probe X-ray microanalysis: techniques and recent applications in biology. *Biol. Rev.*, Vol. 56, pp. 409–461.

Morgan, A.J., 1985. *X-ray Microanalysis in electron microscopy for Biologists.* Oxford University, London, 79 pp.

Mulcahy, S.A., J.S. Killingly, C.F. Phleger & W.H. Berger, 1979. Isotopic composition of otoliths from the bentho-pelagic fish, *Coryphaenoides acrolepsi*, Macrouridae Gadiformes. *Ocean. Acta*, Vol. 2, pp. 423–427.

Mulligan, T.J., L. Lapi, R. Kieser, S.B. Yamada & D.L. Duewer, 1983. Salmon stock identification based on elemental composition of vertebrae. *Can. J. Fish. Aquat. Sci.*, Vol. 40, pp. 215–229.

Mulligan, T.J., F.D. Martin, R.A. Smucker & D.A. Wright, 1987. A method of stock identification based on the elemental composition of striped bass *Morone saxatilis* (Walbaum) otoliths. *J. Exp. Mar. Biol. Ecol.*, Vol. 114, pp. 241–248.

Naney, M.T., 1984. A grinding/polishing tool to aid thin section preparation of small samples. *Am. Mineral.*, Vol. 69, pp. 404–405.

Neilson, J.D. & G.H. Geen, 1981. Method of preparing otoliths for microstructure examination. *Prog. Fish Cult.*, Vol. 43, pp. 90–91.

Pannella, G., 1980. Methods of preparing fish sagittae for the study of growth patterns. In, *Skeletal growth of aquatic organisms*, edited by D.C. Rhoads & R.A. Lutz, Plenum Press, New York, 750 pp.

Papadopoulou, C., G.D. Kanias & E. Moraitopoulou-Kassimati, 1978. Zinc content in otoliths of mackerel from the Aegean. *Mar. Poll. Bull.*, Vol. 9, pp. 106–108.

Papadopoulou, C., G.D. Kanias & E. Moraitopoulou-Kassimati, 1980. Trace element content in fish otoliths in relation to age and size. *Mar. Poll. Bull.*, Vol. 11, pp. 68–72.

Papadopoulou, C. & E. Moraitopoulou-Kassimati, 1977. Stable elements in skeletal formations of fish species from Greek waters. *Thalassia Jugosl.*, Vol. 13, pp. 187–192.

Philibert, J., 1963. A method for calculating the absorption correction in electron probe analysis. In, *Proc. 3rd Int. Conf. X-ray Opt. Microanal.*, Academic Press, New York, pp. 379–392.

Potts, P.J., 1987. Electron probe microanalysis. In, *A Handbook of silicate rock analysis, Chapter 10*, Blackie Press, pp. 326–382.

Pouchou, J.L. & F. Pichoir, 1984. A new model for quantitative X-ray microanalysis. *Recer. Aerosp.*, Vol. 3, pp. 167–192.

Radtke, R.L., 1984a. Cod fish otoliths: information storage structures. In, *The propagation of cod Gadus morhua L. Flodevigen Rapp.*, Vol. 1, pp. 273–298.

Radtke, R.L., 1984b. Formation and structural composition of larval striped mullet otoliths. *Trans. Am. Fish. Soc.*, Vol. 113, pp. 186–191.

Radtke, R.L., 1987. Age and growth information available from the otoliths of the Hawaiian snapper, *Pristipomoides filamentosus*. *Coral Reefs*, Vol. 6, pp. 19–25.

Radtke, R.L., 1989. Strontium-calcium concentration ratios in fish otoliths as environmental indicators. *Comp. Biochem. Physiol.*, Vol. 92A, pp. 189–193.

Radtke, R.L., G.M. Cailliet, 1984. Age estimation and growth of the gray reef shark *Carcharhinus amblyrhynchos* from the northwestern Hawaiian Island. *Proc. Res. Inv. NWHI*, Vol. 84–01, pp. 121–127.

Radtke, R.L. & B. Morales-Nin, 1989. Mediterranean juvenile bluefin tuna: life history patterns. *J. Fish Biol.*, Vol. 35, pp. 485–496.

Radtke, R.L. & T.E. Targett, 1984. Rhythmic structural and chemical patterns in otoliths of the Antarctic fish *Notothenia larseni*: their application to age determination. *Polar Biol.*, Vol. 3, pp. 203–210.

Radtke, R.L., T.E. Targett, A. Kellermann, J.L. Bell & K.T. Hill, 1989. Antarctic fish growth: profile of *Trematomus newnesi*. *Mar. Ecol. Prog. Ser.*, Vol. 57, pp. 103–117.

Radtke, R.L. & D.F. Williams & P.C.F. Hurley, 1987. The stable isotopic composition of bluefin tuna (*Thunnus thynnus*) otoliths: evidence for physiological regulation. *Comp. Biochem. Physiol.*, Vol. 87A, pp. 797–801.

Reed, S.J.B., 1975. *Electron microprobe analysis*. Cambridge University Press, Cambridge, 40 pp.

Reed, S.J.B. & N.G. Ware, 1972. Escape peaks and internal fluorescence in X-ray spectra recorded with lithium drifted silicon detectors. *J. Phys. E Sci. Inst.*, Vol. 5, pp. 582–584.

Rosenberg, G.D., 1980. An ontogenetic approach to the environmental significance of bivalve shell chemistry. In, *Skeletal growth of aquatic organisms*, edited by D.C. Rhoads & R.A. Lutz, Plenum Press, New York, pp. 133–168.

Russ, J.C., 1984. *Fundamentals of energy dispersive X-ray analysis*. Butterworths, New York, 308 pp.

Sauer, G.R. & N. Watabe, 1989. Temporal and metal-specific patterns in the accumulation of heavy metals by the scales of *Fundulus heteroclitus*. *Aquat. Toxicol.*, Vol. 14, pp. 233–248.

Schamber, F.H., N.F. Wodke & J.J. McCarthy, 1977. Least squares fit with digital filter; the method and its application to EDS spectra. In, *Proc. 8th Int. Conf. X-ray Opt. Microanal.*, edited by D.R. Beaman, Pendell Publishing Company, Midland, Michigan, pp. 124–132.

Schneider, R.C. & S.V. Smith, 1982. Skeletal Sr content and density in *Porites* spp. in relation to environmental factors. *Mar. Biol.*, Vol. 66, pp. 121–131.

Smith, D.G.W. & S.J.B. Reed, 1981. Rare earth determinations by energy-dispersive electron microprobe techniques. *Inst. Phys. Conf.*, Vol. 61.

Smith, S. V., R. W. Buddemeier, R. C. Redalje & J. E. Houck, 1979. Strontium-calcium thermometry in coral skeletons. *Science*, Vol. 204, pp. 404–407.

Statham, P. J., 1977. Deconvolution and background subtraction by least squares fitting with pre-filtering of spectra. *Analyt. Chem.*, Vol. 49, pp. 2149–2154.

Statham P. J., 1981. X-ray microanalysis with Si (Li) detectors. *J. Microsc.*, Vol. 123, pp. 1–23.

Statham, P. J., 1982. Confidence in microanalysis; lies, damned lies or statistics. In, *Microbeam analysis*, edited by K. F. J. Heinrich, *Proc. 17th Annu. Conf. Microbeam Anal. Soc. Wash. DC*, pp. 1–7.

Thompson, G. & H. D. Livingston, 1970. Strontium and uranium concentrations in aragonite precipitated by some modern corals. *Earth Planet. Sci. Lett.*, Vol. 8, pp. 439–442.

Townsend, D. W., R. L. Radtke, M. A. Morrison & S. D. Folsom, 1989. Recruitment implications of larval herring overwintering distributions in the Gulf of Maine, inferred using a new otolith technique. *Mar. Ecol. Prog. Ser.*, Vol. 55, pp. 1–13.

Ware, N. G., 1981. Computer programs and calibration with the PIBS technique for quantitative electron probe analysis using a lithium-drifted silicon detector. *Comput. Geosci.*, Vol. 7, pp. 167–184.

Ware, N. G. & S. J. B. Reed, 1973. Background correction for quantitative electron microprobe analysis using a lithium drifted silicon X-ray detector. *J. Phys. Sci. Inst.*, Vol. 6, pp. 286–288.

Weber, J. N., 1973. Incorporation of strontium into reef coral skeletal carbonate. *Geochim. Cosmochim. Acta*, Vol. 41, pp. 2173–2190.

oven at 40–45 °C for a minimum of 6 h. Otoliths taken from specimens stored in ethanol should be transferred into progressively dilute solutions of ethanol prior to drying, to prevent rapid dehydration and consequent fracturing. After drying, the otoliths are stored in small polyurethane capsules (20 mm long, 9 mm diameter, normally used for embedding purposes in transmission electron microscopy) in a moisture-free cabinet or under vacuum.

Embedding, sectioning and mounting

The procedure for embedding and sectioning sagittae that we used is as follows: (1) An accurately scaled diagram of the distal surface of the otolith is made with a camera lucida on a stereo-dissecting microscope. The position of the primordium must be accurately marked on the diagram. (2) With the otolith oriented dorso-ventrally, the desired plane of analysis in our experiments ran anterior-posterior at the level of the primordium. To achieve a section encompassing this plane, the otolith is fixed firmly upright on its ventral edge to the base of an embedding mould with a drop of quick-drying epoxy resin. We used flat-bottomed polyurethane vials, in diameter slightly greater than the length of the otolith, as moulds. The mould is then filled with a

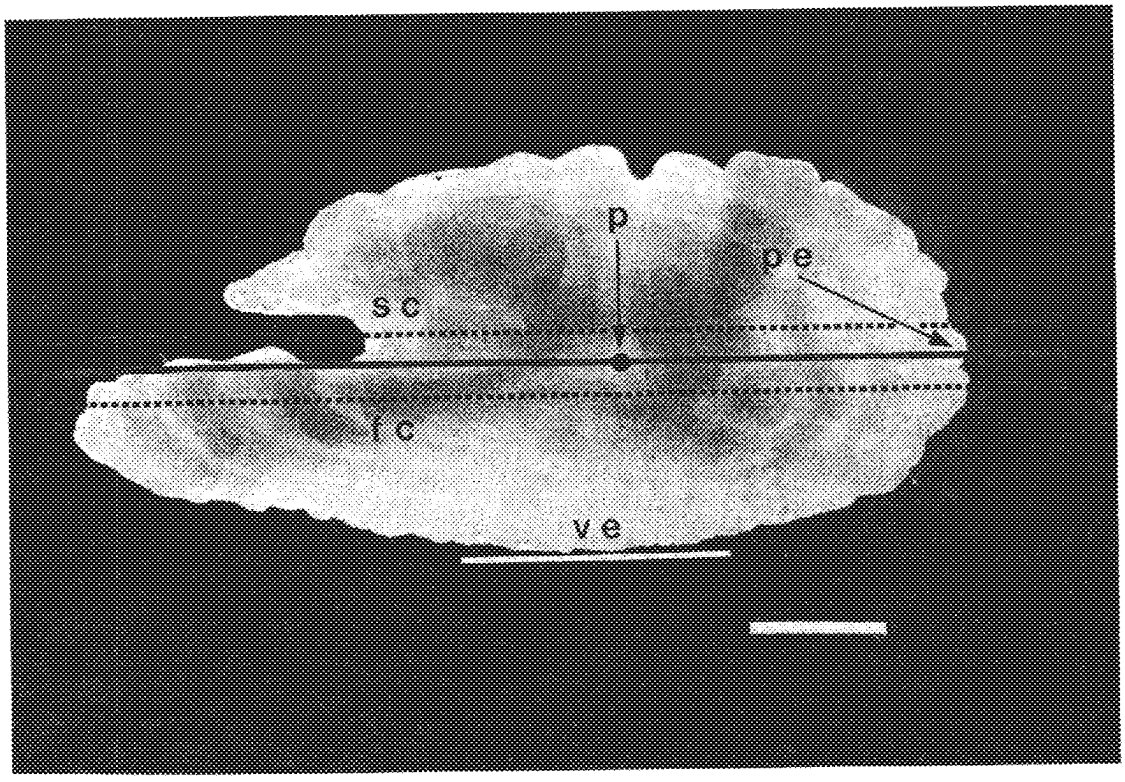

Fig. 1. Distal view of a *N. macropterus* sagitta, showing position of first cut (fc) and second cut (sc) taken to provide a section that includes primordial region (p) and full growth axis to posterior extremity (pe). Solid line at ventral edge (ve) of otolith illustrates region of otolith that is glued to base of mould. Scale bar, 2 mm.

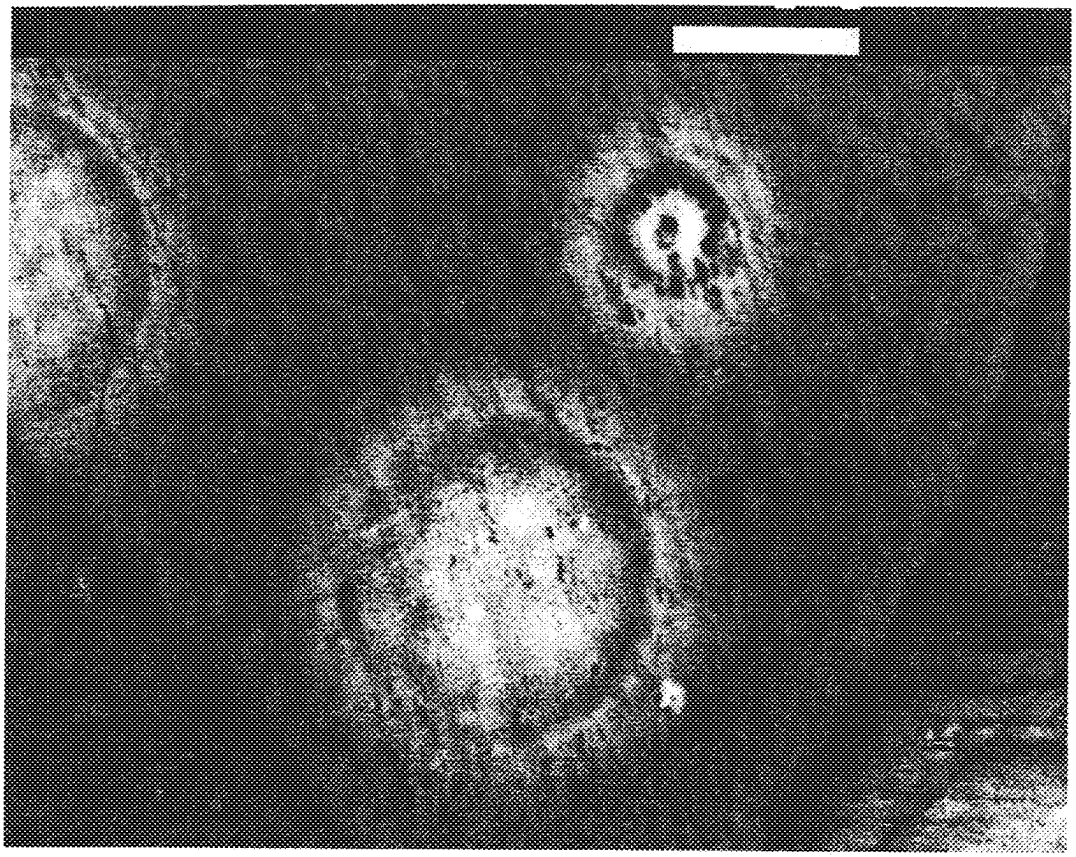

Fig. 5. Backscattered electron micrograph of target regions for two beam conditions on a *N. macropterus* sagitta. Uppermost target is for 14 μm diameter beam at 25 nA and 15 kV; smaller target is for a focussed (<5 μm diameter) beam of same power. Focussed beam produces a central bright region, indicative of extensive decomposition of $CaCO_3$, and severe pitting (black spots around and in target), which may be formed by escaping CO_2.

parameters that define beam power density (E_p, I and A) was varied independently. The number of counts in 5-s intervals were measured over periods of 120 s for Na and 240 s for Sr. Ca was measured on a second spectrometer at the same time as either the Na or Sr counts were being collected. Five replicates of each treatment were taken to estimate the variance in counts between different points in the same region of an otolith.

Experiment 1. The effects of spot size on count rates of Na K_α, Sr L_α and Ca K_α, voltage (15 kV) and beam current (25 nA) held constant; total dwell time 120 s.

Spot sizes ranged in diameter from a nominal 3 μm (focussed beam) to 20 μm (defocussed), which correspond to beam power densities ranging from nominally 50 to 1.2 $\mu W \cdot \mu m^{-2}$. The spot diameter was set by observing the cathodoluminescent disc through the optical microscope of the electron probe when it was targeted on a piece of polished thorium oxide. The effect of spot size on sodium, strontium and calcium counts in successive 5-s intervals is depicted in Fig. 6 and for Na and Sr normalized